MATEMATICAL MODELLING OF MUSSEL GROWTH

Frank Poulsen

IMM-THESIS-2002-31

IMM

MATEMATICAL MODELLING OF MUSSEL GROWTH

Frank Poulsen

IMM-THESIS-2002-31

IMM

ISSN 1601-233x

Trykt af IMM - DTU
Bogbinder Hans Meyer

Preface

This report is carried out at the Institute for Mathematical Modelling (IMM) at the Technical University of Denmark (DTU) in cooperation with the National Environmental Research Institute (NERI) in Denmark. The report also constitutes my Master Thesis in Engineering, the final requirement before my degree.

The author would like the express his gratitude towards the people and institutions which has been very helpfull in contributing data. First of all, I would like to direct thanks to the National Environmental Research Institute in Denmark for providing the detailed mussel samples and the access to the monitoring data for the study area. Especially a thanks to Lars-Ove Loo for providing and pointing out data and report, and for patiently answering my questions. Also, thanks to Kristineberg Marine Research Station in Sweden for providing the detailed meteorological data for the area.

I would also like to thank the Swedish Meteorological and Hydrological Institute (SMHI) for letting me gain access to their SHARK database, which supplied my with monthly values for the sourrounding water bodies. I also greatly appreciated the windspeed data for Måseskär in the period when I was missing windspeed data, and for sending a report on the sediment composition in Havstensfjorden.

Thank you to the people at the 'Skärgårdsproject', who put in a lot of effort to find data for the regional treatment plant in Lungskile.

Also, I am in debt to the people behind the GOTM-model, for making their model publicly available. Without their model, the workload of this report would have increase markedly.

Finally, I would like to thank my advisors, Per Grove Thomsen at IMM, DTU and Jens Kjerulf Petersen at NERI for their advice. Also, I would like to thank you both for giving me the opportunity to work on this project.

Abstract

A mathematical model comprised of 3 coupled submodels (a physical, a biological and mussel model) was developed and compared to observations. The model was then tested for its explainability and value as a management tool.

An ANOVA analysis on 70613 mussel samples showed significant, but small (<15%) variation when grouped into depth, line and distance from southend. The model was developed to study the interaction between almost equal weight gain at different depth and the phytoplankton concentration.

The physical and the biological model was compared with measurements. The physical model was only compared to temperature, which makes it diffucult to validate. Furthermore, it was neccassary to relax salinity concentration to nearby monthly measurement, which made it difficult to adequately simulate mixed layer depth. The biological model was compared to observations, and it adequatly simulated timing and magnitude of blooms at 1.5m, however, blooms at 7m depth was underestimated.

The model suggested that the low differences in mussel growth is due to repeated nutrient pulses from the sediment during wind events, combined with mixing of high surface phytoplankton concentration to the lower layers. Together, these two processes forms an almost uniform phytoplankton profile during blooms, consistent with observations. As a major part of mussel weight gain occurs during blooms, this is a reasonable explanation.

The simulated phytoplankton concentrations was used as input to a detailed mussel model. There was almost no variation between 0-2m and 2-4m depth, consistent with the ANOVA results, but mussel grown at 4-6m depth

was significantly smaller. This is presumably due to the underestimation of subsurface phytoplankton blooms.

Finally, the complete model was tested as a management tool. The task was to calculate a maximum depth from a criteria, e.g. minimum weight gain during a year. Using minimum growth should be half that of the maximum surface growth, the model estimated the acceptable depth to approximately 6m. However, the acceptable depth is likely to be deeper due to underestimating of deep phytoplankton blooms.

The mathematical model approach proved valuable, both as an explanatory tool, as well as a management tool. Further refinements would require local salinity profiles and in situ measurements of sediment nutrient release rates.

Nomenclature

Symbol	Description
u	north-bound current
v	east-bound current
S	Salinity
T	Temperature
ρ	Density
k	Turbulent kinetic energy
ϵ	Dissapation
v_t	Eddy diffusivity
p	Pressure
ρ_0	Reference density
f	Coriolis force
v_t'	Specific eddy diffusivity
I	Solar radiation
C_p	Specific heatcontent of water
I_0	Solar radiatino at surface
a	Ligth extinction coefficient
η_1	Ligth extinction coefficient
η_2	Ligth extinction coefficient
P	Shear production
B	Boyancy production
M^2	Shear frequency
N^2	Brunt-väisälä frequency
$c_{\epsilon 1}$	Dissapation constant
$c_{\epsilon 2}$	Dissapation constant
$c_{\epsilon 3}$	Dissapation constant
σ_ϵ	Dissapation constant
c_μ^0	Stability constant
c_μ	Stabillity function
c_μ'	Stabillity function
$\tilde{a}_N$	Boyancy parameter
τ_x^s	Northernly surface stress
τ_y^s	Easternly surface stress
τ_x^b	Northernly bottom stress
τ_y^b	Easternly bottom stress

Symbol	Description
Q_E	Short-wave radiation
Q_H	Latent heat flux
Q_B	Sensible heat flux
z_0^s	Surface roughness length
z_0^b	Bottom roughness length
c_t	Heat flux constant
c_q	Heat flux constant
q_{10}	Relative humidity at 10m
L	Evaporation constant
c_d	Quadratic drag coeeficient
$\|W_{10}\|$	Windspeed at 10m
W_x	Nothernly wind
W_y	Easternly wind
ρ_a	Air density
T_a	Air temperature
T_w	Water temperature
$q_s(T_a)$	Relative humidity in air
$q_s(T_w)$	Relative humidity abova water
es	Relative humidity function
$airp$	Airpressure

Symbol	Description
Phy	Phytoplankton
Zoo	Zooplankton
NO_3	Nitrate
NH_4	Ammonium
P	Phosphorous
POM_z	Particulate organic matter from zooplankton
POM_p	Particulate organic matter from phytoplankton
Sed	Sediment
μ_p	Phytoplankton growth
m_p	Phytoplankton mortality
grz	Zooplankton grazing
Lim_T	Temperature limitation
Lim_{Par}	Solar radiation limitation
Lim_N	Nitrogen limitation
Lim_P	Phosphorous limitation
$temp$	temperature
I_z	Incedent solar radiation
k_z	Extinction coefficient
Lim_{NO_3}	Nitrate limitation
Lim_{NH_4}	Ammonium limitation
μ_z	Zooplankton growth
exc_z	Zooplankton excretion
m_z	Zooplankton mortality

Symbol	Description	Value	Unit
μ_{max}	Maximum phytoplankton growth	1.5	day^{-1}
m_p	Phytoplankton mortality	0.05	–
Q_{10}	Temperature coefficient for phytoplankton	2	–
$temp_0$	Reference temperature	10	C
k_{par}	Solar radiation limitation coefficient	100	W
k_{back}	Background extinction coefficient	0.35	m^{-1}
k_{phy}	Phytoplankton extinction coefficient	0.05	$m^{-1} \cdot (mmol\ N \cdot m^{-3})^{-1}$
k_{NO_3}	Nitrate limitation half coefficient	1	$mmol\ N \cdot m^{-3}$
k_{NH_4}	Ammonium limitation half coefficient	0.7	$mmol\ N \cdot m^{-3}$
ψ	Nitrate inhibition from ammonium	1.5	$(mmol\ N \cdot m^{-3})^{-1}$
k_p	Phosphorous limitation half coefficient	0.1	$mmol\ P \cdot m^{-3}$
$N2P$	Nitrate to phosphorous ratio	16	$mmol\ N \cdot (mmol\ P)^{-1}$
ass	Assimilatino constant	0.8	–
iv	Ivlev coefficient for grazing	0.5	$mmol\ N \cdot m\ -3$
Phy_{min}	Grazing treshold	0.2	$mmol\ N \cdot m^{-3}$
exc_0	Excretion at 0 degress	0.3	–
$Q_{10_{exc}}$	Temperature coefficient for excretion	1.025	–
mor_{Zoo}	Zooplankton quadratic mortality	0.1	–
W_{POM_P}	Settling velocity for phytoplankton POM	0.5	$m \cdot m^{-1}$
W_{POM_Z}	Settling velocity for phytoplankton POM	10	$m \cdot m^{-1}$
r_{rem}	POM remineralisation rate	0.1	–
r_{nit}	Nitrification rate	0.1	–

Symbol	Description	Value	Unit
Mus	Mussel weight		
Mus_{ass}	Mussel assimilation		
Mus_{res}	Mussel respiration		
Ass_{phy}	Phytoplankton assimilation		
Ass_{det}	Detritus assimilation		
Ing_{phy}	Phytoplankton ingestion		
Ing_{det}	Detritus ingestion		
Ing_{silt}	Silt ingestion		
Ing_{SPM}	Suspended particulate matter ingestion		
gut_{RT}	Gut retention time		
$Filt_{Phy}$	Phytoplankton filtration		
$Filt_{det}$	Detritus filtration		
$Filt_{silt}$	Silt filtration		
$Filt_{SPM}$	Suspended particulate matter filtration		
Cle	Clearance rate		
rej	Mussel rejection		
sel	Mussel selection		
GrC	mol C to g DW ratio	30	$g\ DW(mol\ C)^{-1}$
Ing_{Max}	Maximum ingestion rate	$7.9 \cdot 10^{-3}$	$g\ DW \cdot h^{-1} \cdot ind^{-1}$
Rej_{Max}	Maximum rejection rate	0.97	-
$Filt_{Th}$	Treshold for pseudofaces	$7.8 \cdot 10^{-3}$	$g\ DW \cdot h^{-1} \cdot ind^{-1}$
K_{Rej}	Coefficient for rejection	$9.4 \cdot 10^{-3}$	$g\ DW \cdot h^{-1} \cdot ind^{-1}$
Sel_{Max}	Maximum selection coefficient	0.7	-
K_{Sel}	Coefficient for selection	0.01	$g\ DW \cdot h^{-1} \cdot ind^{-1}$
$K_{Ass_{Phy}}$	Coefficient for algae assimilation	0.5	h
$K_{Ass_{Det}}$	Coefficient for detritus assimilation	5	h
Gut_{Vol}	Gut volume	0.01	$g\ DW \cdot ind^{-1}$
Res_{Ba}	Basal respiration	$1.3 \cdot 10^{-4}$	$mol\ C \cdot d^{-1} \cdot ind^{-1}$
Ass_{Cost}	Fraction of assimilation respired	0.04	-

Contents

Chapter 1

Introduction

Mussels are becoming a more and more important food source in the world. In Denmark alone 100.000 t is produced annually. Still, the cultivation is almost exclusively harvest of the natural on-bottom population through means of dredging. Besides the ecological impact, bottom-dwelling mussel are not in direct contact with the high-productive photic zone. Thus, from both an ecological and an economic viewpoint, something could be gained by changing production method.

Traditionally, there has been alternatives for a long time, see e.g Gosling (1992). In India, a pole system has traditionally been used, and in Spain, many mussel are produced on a system, aptly named "Spanish rafts." A more recent technique is the long-line system, where long lines are hung from floaters. All these methods transfer the mussels to the productive zone and avoids dredging. In this report, focus is on the last method: "the long-line system."

Even though the long-line system is not entirely new, not many has studied the design of such a system. It is the aim of this report to attempt to contribute to the knowledge of this system by analysing a longline system in Lungskile, Sweden.

More specifically, mussel samples will be analysed to investigate variation in growth in different sections of the system. Furthermore, mathematical modelling will be used to try and clarify what controls these variations. Furthermore, the models usability as a management tool will be evaluated.

Many models of mussels has been developed for management purposes (see e.g. Beadman et al. (2002) for a recent review), but apparently all for on-bottom natural populations. This model differs from the others by looking specifically at off-bottom mussel cultures instead.

The report will briefly describe the study area and present the available observation, including mussel samples from Lungskile. The mathematical model is split into 3 parts: A physical model, a biological model and a mussel model. Each will be described independently before the model results are presented. Finally, the results are discussed before reaching a conclusion.

Chapter 2

The Study Area

The study area is located in a small bay in the south-west of Sweden, outside the town of Lungskile. The bay is a part of Havstenfjorden, which together with Koljöfjorden, Stigfjorden and Hakefjorden comprises an open-ended fjordsystem. The water circulation is subtidal (tidal amplitude ca. 30 cm in the spring) and counter-clockwise, primarily forced by a salinity gradient between the low saline Baltic water and Skagerrak (Björk et al., 2000)).

Havstensfjorden has a surface area of approximate 61 km^2 and the mean retention time is estimated to 80d, making the primary production local (Björk et al., 2000)). The water depth at the study area is 12m (see data) and the sediment is characterized as silt-clay, an active bottom fauna without indication of hypoxia and a mean depth of RPD (Redox Potential Discontinuity) of 2.1 cm (Nilsson and Rosenberg, 1997)). Sediment samples in 1975 measured 3.5 g/kg Total Nitrogen, and samples in 1995 measured a sligth increase to 3.6 g/kg Total Nitrogen. The Phosphorous concentration was measured in 1995, at a concentration of 0.96 g/kg Total Phosphorous (Ingemar, 1997).

Known point sources for nutrients are primarily the regional treatment plant in Lungskile and secondary sources are treatment plants on Tjörn and in Stenungssund, as well as the chemical industry in Stenungssund Lann and Oscarson (2000)). The release rates from the Lungskile regional treatment plant is presented in table 2.1. The secondary nutrient inputs are transferred from Hakefjorden to Havstensfjorden with the dominant current

Björk et al. (2000)). The nutrient loading in the area is also reflected in a gradient in winter values increasing from the coastal waters towards Havstensfjorden Lann and Oscarson (2000)).

Year	N-tot	P-tot
1996	16.1	0.273
1998	14	0.122
1999	11	0.057
2000	10.13	0.09
2001	9.13	0.08

Table 2.1: Release of nutrient from the Lungskile regional treatment plant in T/year

Chapter 3

Observations

3.1 Mussels

During 10 sampling dates between the 23rd of August 1999 and 29th of October 2000, 358 samples of 1m of line from a mussel culture in Lungskile was analysed. A total of 70613 mussels was measured for individual length and 1158 mussels were measure for meat and shell dry weigth (mg). All samples was classified according to 10 lines, 10 meter intervals from the south end and 3 depths from 0 to 6m.

From these samples, 5 parameters were calculated: Number, Length, Condition index, Weigth and Biomass. Number and Length were already provided from the sampling data, and a regresion using equation 3.1 was used to convert length into weight, where b is the Condition index. A summery of all the individual weigths in a sample yields the biomass for 1m line.

$$weigth = a \cdot length^b \tag{3.1}$$

3.1.1 Depth

To clarify differences between depth, an ANOVA analysis was conducted for biomass, length, weight and number. A post-hoc Tukey-Kramer test was

Depth	biomass	length	weigth	number
$0-2m$	2.18	-0.85	$+1.0$	-1.5
	(+6.4%)	(-3.9%)	(5.8%)	(0%)
$2-4m$	-2.81	0.31	-0.8	-43.8
	(-8.3%)	(+1.4%)	(-4.4%)	(-1.9%)
$4-6m$	0.88	0.54	-0.2	47.6
	(+2.6%)	(+2.4%)	(-1.0%)	(2%)

Table 3.1: ANOVA analysis of biomass means

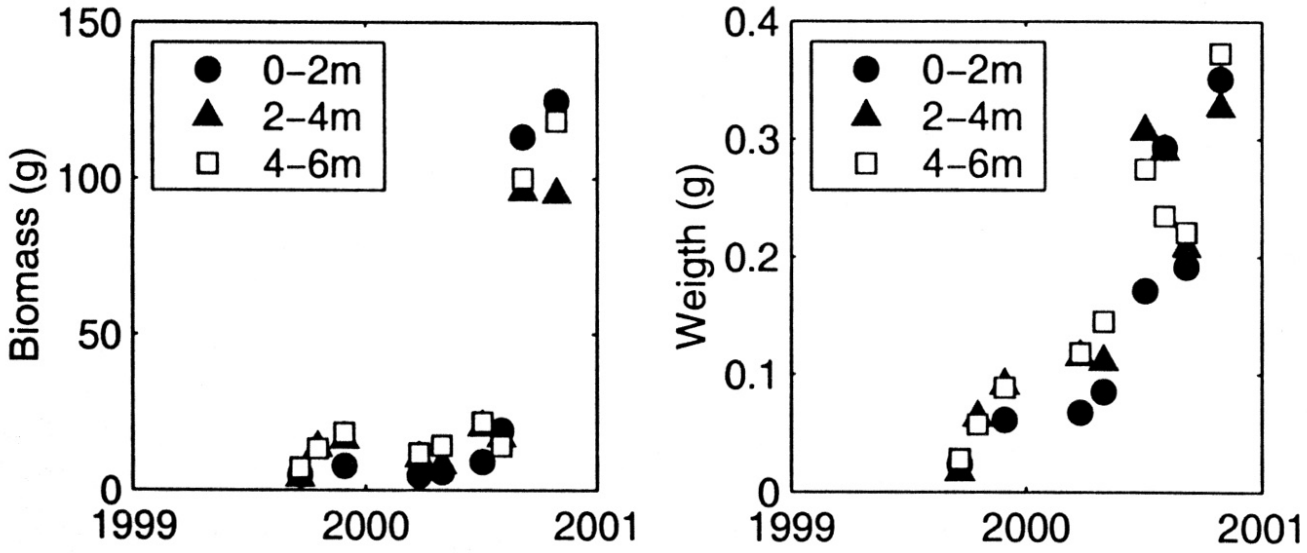

Figure 3.1: Mean mussel biomass and weigth for 3 depth

performed to determine if the differences was significant. The differences from mean values for the three depth a summerized in table 3.2.

The biomass analysis revealed that the mean biomass at 2-4m depth was significantly lower than 0-2m (95%) and 4-6m(90%). However, there was no significant difference between 0-2m and 4-6m (< 75). Note that the differences are relatively small compared with the mean biomass ($33.99g \cdot m^{-1}$).

All length means for the different depth are significantly ($> 75\%$) different, however the variations are relatively small ($< 4\%$ diviation from overall mean). The mussel length is shorter at the surface (0-2m) than lower (2-4m and 4-6m).

For individual mussel weight, intersample variations are larger than date and depth variations, which can be seen from an ANOVA R-squared fit of

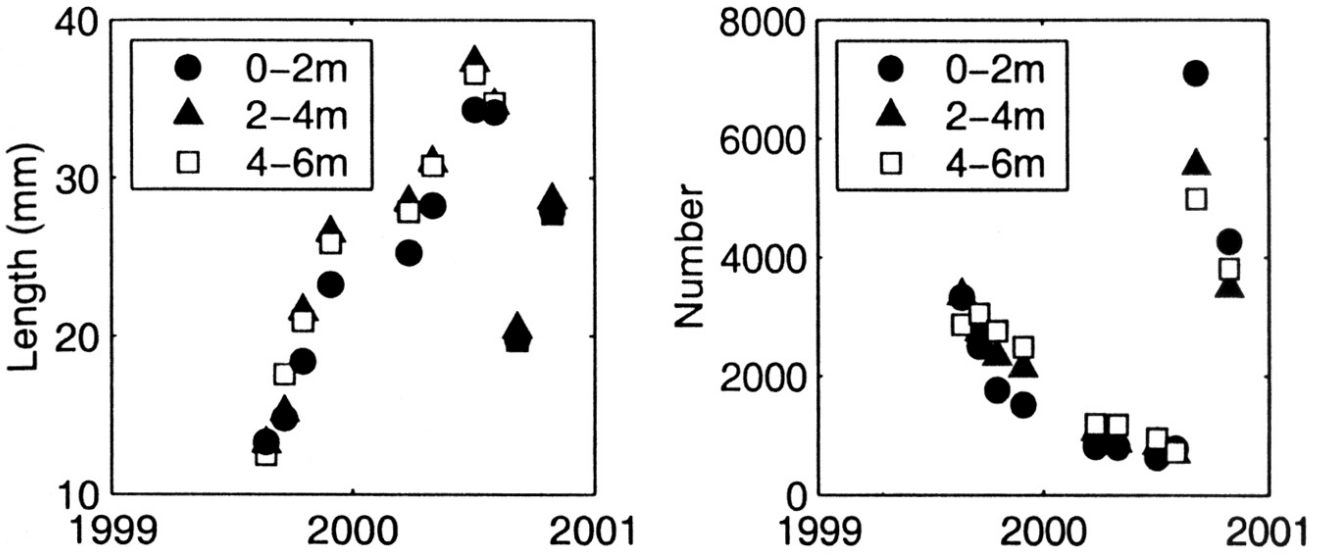

Figure 3.2: Mean mussel length and number for 3 depth

Line	length	weigth	number
$1-3$	+0.47	-8.1	-26.4
	(+2.1%)	(-4.5%)	(-13.3%)
$4-7$	-0.60	-3.4	+21.2
	(-2.7%)	(-1.9%)	(+10.7%)
$8-10$	+0.68	+16.1	-2.4
	(+3.1%)	(+9.0%)	(-1.2%)

Table 3.2: ANOVA analysis of biomass means

only 5.8%. The mean weigth is 178 mg, and variations are around 10mg or $5-6\%$. Here, the mussel in the surface is on average 1 mm above mean, with lower located mussel being slightly shorter than mean.

The number of mussel on 10 m line is not significantly ($< 75\%$) different between depth.

3.1.2 Line

Note that the ANOVA is no longer balanced, as there are a different number of samples for the three groups. There were 20180 samples from line 1-3, 34119 from line 4-7 and line 8-10 was sampled 16314 times. Furthermore, biomass can not be studied by line because of the regressions are not divided into lines.

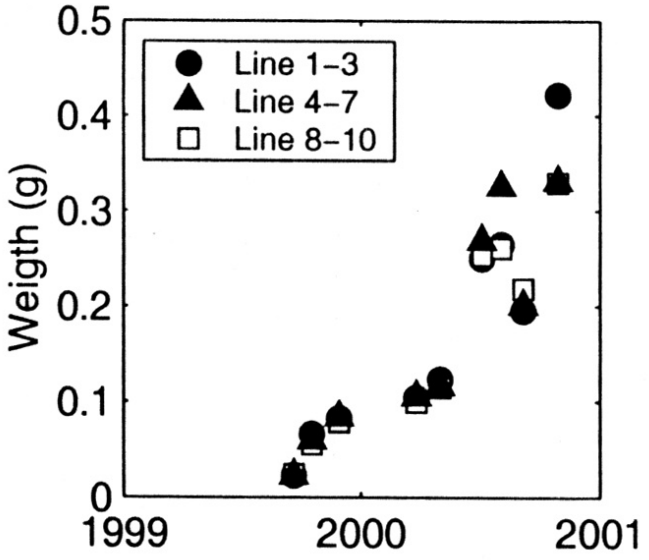

Figure 3.3: Mean mussel for 3 groups of lines

Length differences between lines 1-3 and 8-10, as well as between lines 4-7 and 8-10 is very significant (>95%). Differences between lines 1-3 and 8-10 are also significant on a >90% level. However, the differences are low (< 4%).

The R-squared for weigth is only 0.06, which indicates that variations within a sample is larger than between samples. The differences between lines 1-3 and 8-10, as well as between lines 4-7 and 8-10, is significant at a confidence level of 95%. However, differences between lines 1-3 and 4-7 is insignicant at a level of 50%.

Differences in numbers between lines 1-3 and 4-7 is highly significant (>95%). All other number differences is significant on an 90% level.

There is no clear pattern in line differences for any of the parameters. Some differences may be significant, but all differences are below 11%.

3.1.3 Distance from south end

For length, the R-squared is 0.32 and all differences between means are significant on a 95% level. The reason that the nothern length (at a distance of more than 300m from the southend) is so large compared to the other means should probably be found in the sampling dates, as this distance is only sampled in 2000, whereas the other distances are samples in 1999 as well.

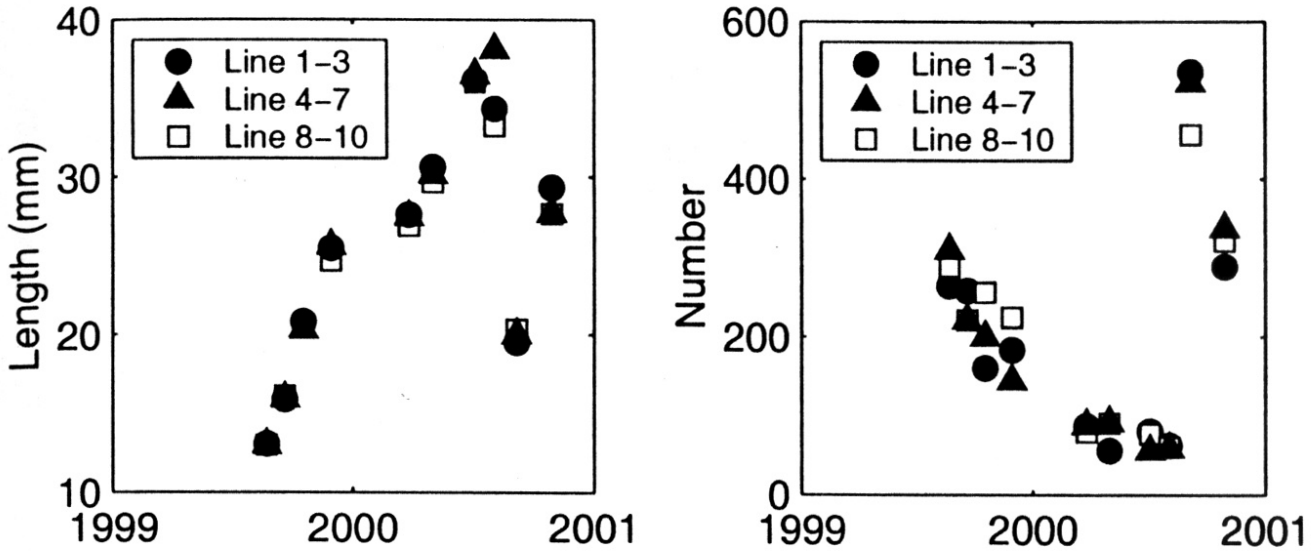

Figure 3.4: Mean mussel length and number for 3 groups of lines

Distance from southend	length (cm)	weigth (mg)	number
$< 100m$	-0.19	-11.9	+4.8
	(-0.8%)	(-6.7%)	(+2.4%)
$100 - 300m$	-0.66	+3.8	+15.8
	(-3.8%)	(2.1%)	(+7.9%)
$> 300m$	+5.82	+25.7	-79.0
	(+26.3%)	(+14.4%)	(-39.7%)

Table 3.3: ANOVA analysis of biomass means

The ANOVA for weigth has a very low R-squared (>0.06) and all differences between means are very significant (>95%). Again, the variations within a sample is larger than between dates and distances.

Number of mussel on the last 100 meters north (distance from southend>300m) is significantly lower than the rest of the culture. Again, remember that this distance is only sampled in 2000, where many of the mussel shave falled off. Difference between the first 100m and the middle part of the culture is insignificant at the 75% level.

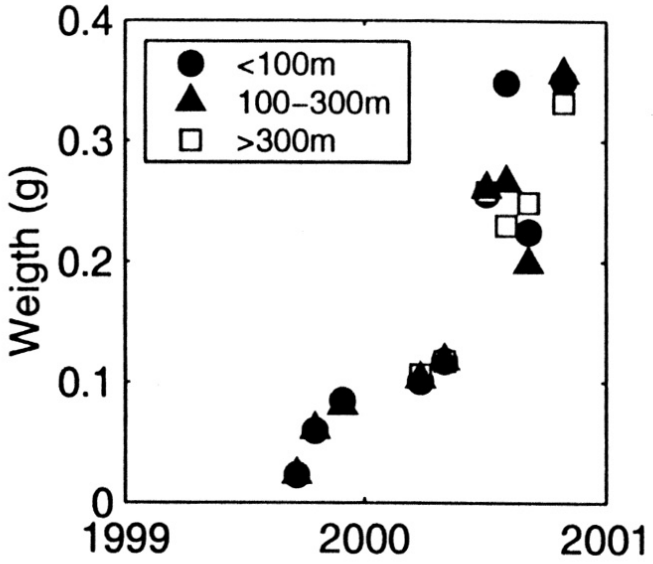

Figure 3.5: Mean mussel for 3 groups of distance from south end

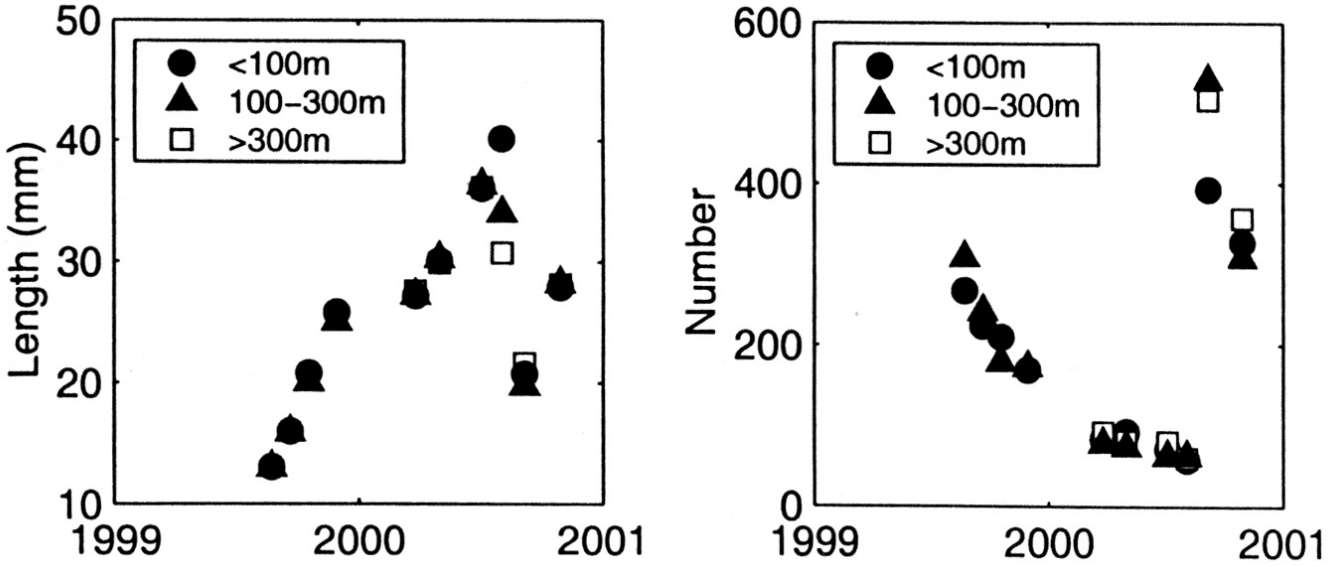

Figure 3.6: Mean mussel length and number for 3 groups of distances from south end

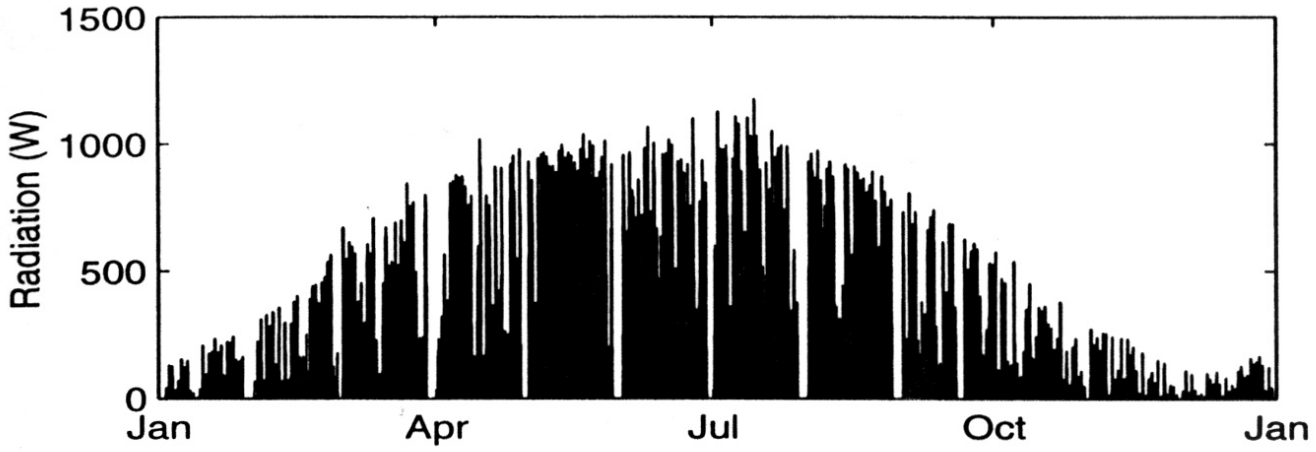

Figure 3.7: Incident radiation

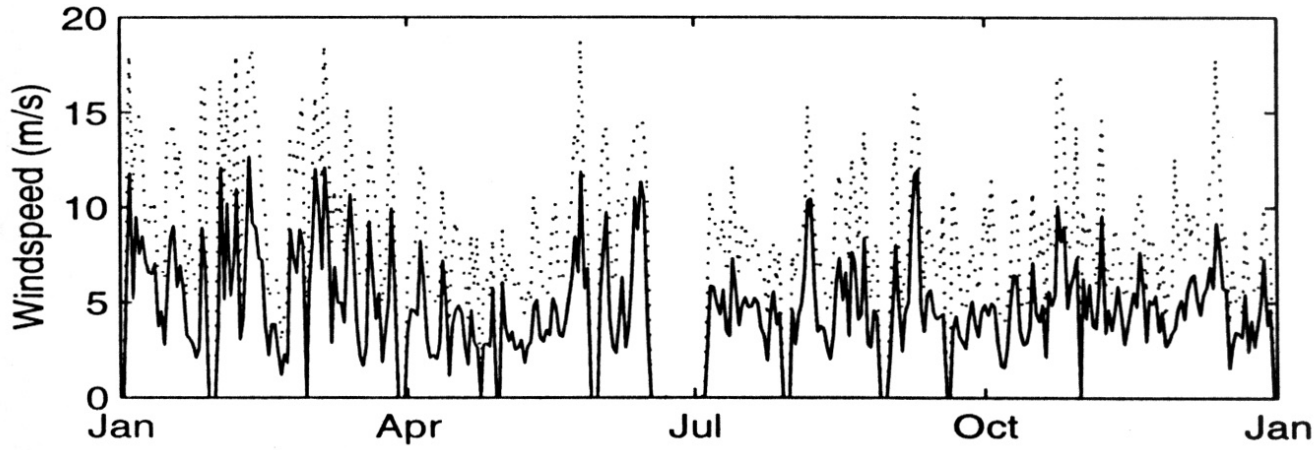

Figure 3.8: Average and maximum daily windspeeds [Solid line: mean daily windspeeds, Dotted line: Max daily windspeeds]

3.2 Meteorological data

The meteorological data used in this study is obtained from Kristineberg meteorological station. The data consist of time series of solar radiation, windspeed and -direction and airtemperature and -pressure, all measured at five minute intervals. Solar radiation and wind speed is presented in figure 3.7 and 3.8 respectively. Wind speed measurements are missing from the 16th of June to the 5th of July due to failure of the windsensor. Instead, data from Måseskär, sampled every 3 hours, is used. Missing data in short time scales (days) are generated by time series analysis. Note the wind events apparent in June, August and September, all with average daily windspeeds reaching more than 10 m/s.

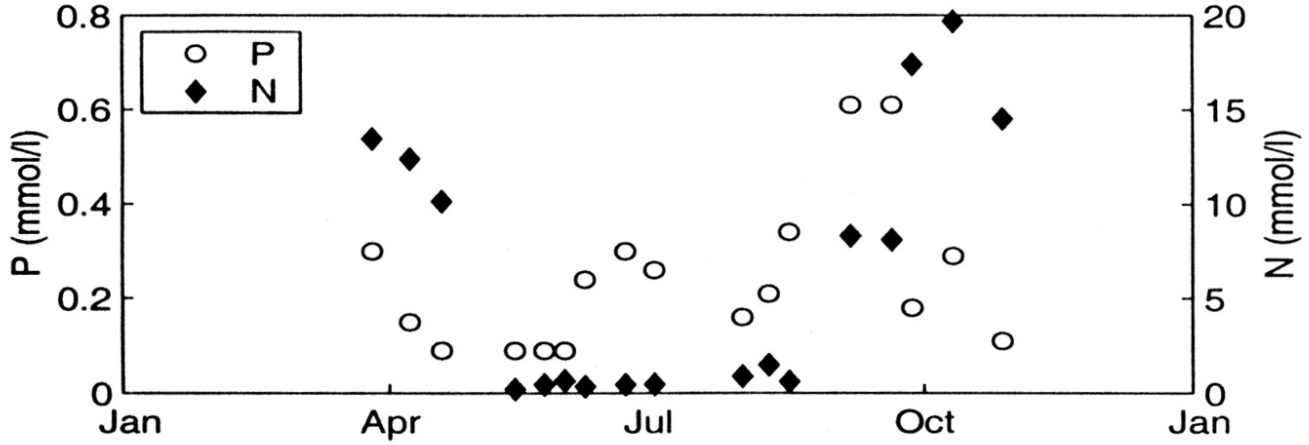

Figure 3.9: Measured Phosphorous and Nitrate+Ammonium at 1.5m depth

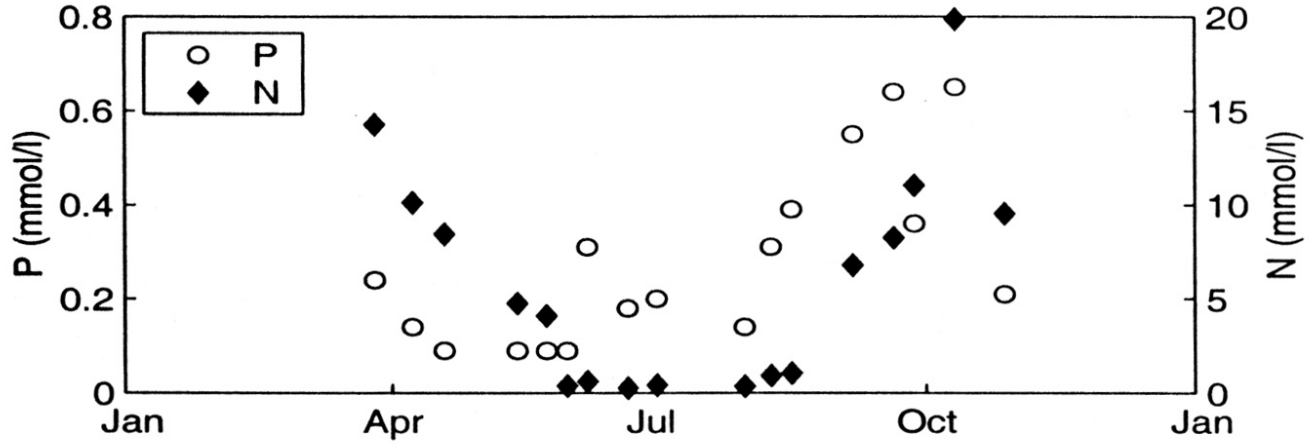

Figure 3.10: Measured Phosphorous and Nitrate+Ammonium at 7m depth

3.3 Nutrients

Nutrients are measured in two depth (1.5m and 7m) at intervals of 1-3 weeks from the 26th of March to the 28th of October. The measured nutrients are Phosphorous (PO_4-P), Nitrate (NO_3-N), Ammonium (NH_4) and Silicium (SiO_3-Si). Figure 3.9 and 3.10 show the measured values for Phosphorous and Nitrate+Ammonium in the two depth. Phosphorous values at 0.1 mmol/l is not actually measured values, but represent no detectable Phosphorous, with a detection limit 0.1 mmol/l. Measurements were also conducted during a campaign from the 10^{th} to the 20^{th} of July 2000. To avoid clottering, these values are not shown in figure 3.9 and 3.10 as daily values is not well presented on an annual time scale.

For both depths, Phosphorous is depleted before Nitrate, but depletion of

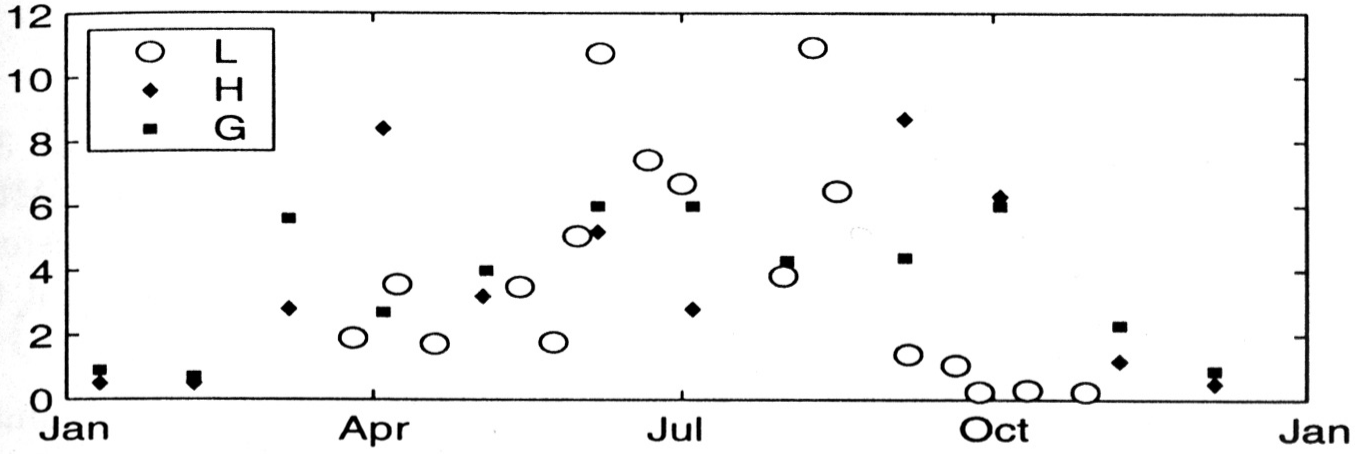

Figure 3.11: Observed phytoplankton at 1.5m depth [L=Lungskile, H=Havstensfjorden, G=Galterö

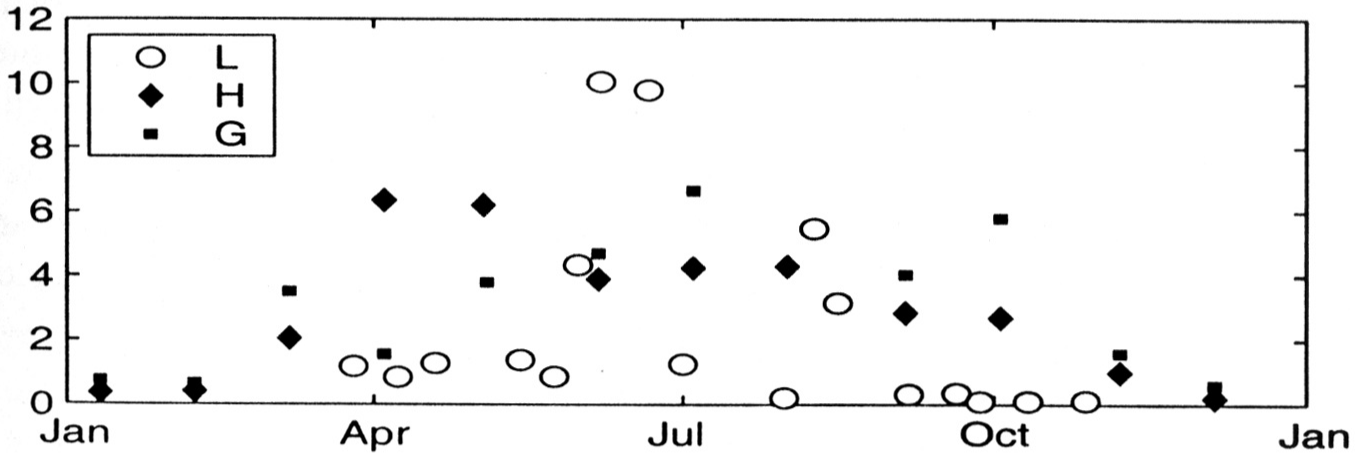

Figure 3.12: Observed phytoplankton at 7m depth [L=Lungskile, H=Havstensfjorden, G=Galterö

the nutrients occur a little later at 7m depth than at 1.5m. To evaluate which nutrient is limiting, the Redfield-ratio ($12\ mmol\ N \cdot (mmol\ P)^{-1}$) is used, assuming that P is limiting if the N to P ratio is above the Redfield-ratio. Accordingly, P is limiting before 19^{th} of April and again after the 20^{th} of September. At 7m depth, Phosphorous is also limiting on the 6^{th} of September. Thus, the system changes between P-limitation in spring and autumn and N-limitation during summer.

3.4 Phytoplankton

Chl a is sampled concurrently with the nutrients presented in section 3.3. Furthermore, the Swedish Meteorological and Hydraulic Institute (SMHI) conducts a monitoring program called SHARK, which samples Havstensfjorden and Galterö once every month. Figure 3.11 and 3.12 present the collected measurements.

According to Edler (2000), the bloom begins in March, when the number of diatom species increase rapidly. This is before the sampling begins at Lungskile, so the bloom is not visible in the Lungskile data. The spring values for Havstensfjorden and Galterö presumably depends on whether the sampling date coincides with the spring bloom. The observations for Lungskile shows 2 peaks after April, Havstenfjorden exhibits a autumn bloom and Galterö apperently only has a spring bloom. However, peaks can occur between sampling dates and conclusions can not be drawn on such sparse data.

An obvious differences between Lungskile and the two surrounding areas are the autumn/winter values. September and October samplings are considerably lower in Lungskile compared to Havstenfjorden and Galterö. In fact, the values in Lungskile are below winter values for the area.

Chapter 4

Model descriptions

4.1 The Physical Model

This section describes the physical model. Consistent with the primary objective, it is out of the scope of this paper to develop a full physical model. Furthermore, there is no need to develop a new model, a several excellent models already exists. This section describes a physical model called GOTM (General Ocean Turbulence Model). The choice of GOTM is adressed in section 4.1.1. Before the variables and equations are presented, the choice of model is discussed and the selected model is placed in a wider frame, e.g. type of turbulens equations. The effects of the equations are then explained before the boundary and forcing equations are presented. Finally, before the results can be presented and validated, the inital values are discussed and the choice of model settings is referred.

4.1.1 Choice of model

To select an appropriate model, it was decided to set up a list of criterias the model should fullfil. The chosen criterias are:

- Well-documented
- Validated
- Simple to use

- Simple to install

The most common models of turbulence encountered in literature is the k-ϵ and the Mellor-Yamada equations. In a study by Burchard and Petersen (1999), they concluded that both models adequately and similarly models mixing due to heating, cooling, wind and bottom shear stress. Similarly, Chen and Annan (2000) studied the ecosystem response to different mixing model. Their conclusion was the same as Burchard and Petersen (1999), that all models yielded physically realistic results, except from the simplest Mellor-Yamada model (level 2). However, they found that the choice of turbulent closure scheme significantly influenced the timing and depth of the blooms, the strength and position of the subsurface maximum and the total integrated primary production.

The GOTM model implements the k-ϵ equations and it is considered able to fullfil the criterias presented earlier. A detailed report (Burchard et al., 2000) accompanies the model and it has been validated in a wide variety of situations, see table 4.1. Furthermore, it is easy to use and several pre-compiled versions can be downloaded from the Internet (www.gotm.net). In this study, GOTM version 2.2.5 is used.

The description of the state variables and the governing equations (sections 4.1.2 and 4.1.3) are based on the provided GOTM documentation (Burchard et al., 2000), and supplemented by an article which details the equations of the Mellor-Yamada and k-ϵ models (Burchard and Petersen, 1999), coauthored Hans Buchard, one of the developer of GOTM.

4.1.2 State variables

The physical model has 6 properties, which can be divided into 3 categories: Hydrodynamic, tracer and turbulent properties. This division is based on their use in the relevant equations. The hydrodynamic properties are the current speed in the north- and eastbound direction, u and v, and they are both measured in m/s. The tracer properties are salinity in ppt (S) and temperature in celsius (T), which also defines the density (ρ), calculated from S and T by the UNESCO formula. Later, in the biological model, more tracers will be added. Finally, the turbulent properties are turbulent kinetic energy (k) and dissapation of kinetic energi (ϵ), measured in m^2/s^2 and m^2/s^3.

Case name	Description	Depth	Time period
Liverpool Bay	Tidal straining in Liverpool Bay (UK) 53.47N, 3.65W	32m	33h
Provess	Mixing in Northern North Sea 59.33N, 1.28E	110m	20d
Flex	North Sea (Fladenground) 58.55N, 0.32E	145m	74d
Irish Sea	Irish Sea 53.49N, 5.27W	90m	1d
Knebel Vig	Fjord (Denmark) 56.10N, 10.27E	11m	2d
Ooster Schelde	Zeeland (Netherlands) 51.33N, 3.54E	12m	3d
OWS November	Pacific Subtropical 30N, 140W	>250m	10y
OWS Papa	Pacific North 50 N, 145 W	>250m	22y
Lago Maggiore	Convective mixing in Lago Maggiore (Italy) 45.82N, 8.6E	42m	3d
Umlauf-Burchard	Surface wave breaking after Umlauf and Burchard.	10m	5d
Kato-Philipps	Mixed layer deepening under constant boyancy flux.	50m	30h
Couette	Steady-state channel flow driven by surface stress.	10m	12h
Channel	Steady-state channel flow forced by external pressure gradient only.	10m	12h
Convection	Penetration of a mixed layer into stratified flow due to negative heat flux.	40m	3d
Estuary	Estuarine circulation forced by internal and external pressure gradients.	15m	10d
Rouse	Sediment-laden steady-state channel flow for reproducing the Rouse profile.	10m	2d
Craig-Banner	Surface wave breaking after Craig and Banner.	50m	5d

Table 4.1: Test cases for the GOTM model

4.1.3 Equations

The hydrodynamic advection-diffusion equations are calculated from vertical diffusion, the (internal and external) pressure gradient and the Coriolis rotation, see equation 4.1 and 4.2.

$$\partial_t u - \partial_z(v_t \partial_z u) = -\partial_x \frac{p}{\rho_0} + f \cdot v \tag{4.1}$$

$$\partial_t v - \partial_z(v_t \partial_z v) = -\partial_y \frac{p}{\rho_0} - f \cdot u \tag{4.2}$$

The vertical diffusion is related to the turbulent properties, which will be described later. Tidal flow is included in the external pressure gradient, however it is neglected in the current use of GOTM as the tide is low, in the maximum range of 30cm (Björk et al., 2000). The location of the simulated area defines the last contribution, the Coriolis rotation.

The tracer equations are determined by the general tracer equation, internal source and sink terms and the boundary conditions. The general one-dimensional equation for a tracer X is shown in equation 4.3 and the boundary conditions are treated in a section 4.1.5. The diffusivity is split into a molecular diffusivity, specific for the tracer, and eddy diffusivity, calculated from the turbulent properties.

$$\partial_t X - \partial_z((v_t + v_t') \cdot \partial_z X) = R(X) \tag{4.3}$$

The specific molecular diffusivity is $1.4 \cdot 10^{-7} m^2 \cdot s^{-1}$ for temperature and $1.1 \cdot 10^{-9} m^2 \cdot s^{-1}$ for salt. No inner source or sink terms for salinity are assumed in GOTM, and boundary salinity fluxes (e.g. precipitation and evaporation) is ignored, making salinity a conservative tracer. The significance of this assumption is further studied in section 5.1.3.

Inner sources for temperature is incoming short-wave radiation, which is being converted to heat by absortion in the water column, and is modelled by equation 4.4. The available radiation in a specific depth is modelled according to equation 4.5 and ligth attenuation is calculated from a specified Jerlov type.

$$R(T) = \frac{\partial_z I}{C_p \cdot \rho_0} \tag{4.4}$$

$$I(z) = I_o(a \cdot e^{-\eta_1 \cdot z} + (1-a) \cdot e^{-\eta_2 \cdot z}) \tag{4.5}$$

Now, only the turbulent properties need to be defined to close the system. These are, however, more complicated than the hydrodynamic and tracer properties. Turbulent kinetic energi (k) increases with shear production (P) and decreases with boyancy production (B) and dissapation (ϵ). Furthermore, the turbulent kinetic energy is exchanged between layers by diffusion, see equation 4.6. To include internally breaking waves, which is not explicitly modelled in GOTM, a minimum turbulent kinetic energy of $3 \cdot 10^{-6} m^2 \cdot s^{-1}$ is applied.

$$\partial_t k - \partial_z(v_t \partial_z k) = P + B - \epsilon \tag{4.6}$$

Shear production (P) is a product of shear frequency (M^2) and eddy viscosity (v_t), and the shear frequency increases with the current speed gradient, see equation 4.7 and 4.8.

$$P = v_t \cdot M^2 \tag{4.7}$$

$$M = \sqrt{(\partial_z u)^2 + (\partial_z v)^2} \tag{4.8}$$

The turbulent kinetic energy is decreased by boyancy production, a function of eddy diffusivity and the Brunt-Väisälä frequency, which is dependent on the density gradient. The two formulations of the two processes are shown in equation 4.9 and 4.10.

$$B = -v_t' \cdot N^2 \tag{4.9}$$

$$N^2 = -\frac{g}{\rho_0} \partial_z \rho \tag{4.10}$$

Finally, the turbulent kinetic energy is removed by dissapation (ϵ), which equation resembles the equation for k, except for the addition of an ϵ/k

factor and 3 constants, see equation 4.11. To include the limiting effect of stable stratification, a maximum turbulent length scale is applied, which in a k-ϵ model corresponds to a lower limit to the dissapation rate, see equation 4.12.

$$\partial_t \epsilon - \partial_z (\frac{\nu_t}{\sigma_\epsilon} \partial_z \epsilon) = \frac{\epsilon}{k} (c_{\epsilon 1} \cdot P + c_{\epsilon 2} \cdot B - c_{\epsilon 3} \cdot \epsilon) \tag{4.11}$$

$$\epsilon^2 \geq 0.045 \cdot k^2 \cdot N^2 \tag{4.12}$$

To close the turbulence equation and to calculate the diffusion terms of the hydrodynamic and tracer equation, the eddy viscosity (ν_t) and eddy diffusivity (ν_t') needs to be calculated. They are both based on a stability function (c_μ and c_μ'), the square root of the turbulent kinetic energy ($\sqrt{k}$) and a turbulent length scale (L), calculate from k and ϵ. The stability functions are calculated from a non-deminsional boyancy parameter ($\tilde{a}_N$) shown in equation 4.15, and they are presented in equation 4.13 and 4.14. The turbulent length scale L is shown in equation 4.16 and the equations for ν_t and ν_t' are number 4.17 and 4.18.

$$c_\mu = \frac{c_\mu^0 + 2.182 \cdot \tilde{a}_N}{1 + 20.40 \cdot \tilde{a}_N + 53.12 \cdot (\tilde{a}_N)^2} \tag{4.13}$$

$$c_\mu' = \frac{0.6985}{1 + 17.34 \cdot \tilde{a}_N} \tag{4.14}$$

$$\tilde{a}_N = \frac{L^2}{k} N^2 \tag{4.15}$$

$$L = (c_\mu^0)^3 \cdot \frac{k^{3/2}}{\epsilon} \tag{4.16}$$

$$\nu_t = c_\mu \cdot \sqrt{k} \cdot L \tag{4.17}$$

$$\nu_t' = c_\mu' \cdot \sqrt{k} \cdot L \tag{4.18}$$

The constant used in GOTM is presented in table 4.2.

$c_{\epsilon 1}$	$c_{\epsilon 2}$	$c_{\epsilon 3}(B<0)$	$c_{\epsilon 3}(B>0)$	σ_ϵ	c_μ^0
1.44	1.92	−0.4	1.0	1.08	0.5562

Table 4.2: GOTM constants

4.1.4 Boundary conditions

The surface boundary conditions for the hydrodynamic properties (u and v) are given by the surface stress τ^s, see equation 4.19 and 4.20. The calculation of the surface stress is adressed in the section 4.1.5. For the bottom boundary condition, a no-slip condition is assumed, so u and v is zero at the bottom (equations 4.21 and 4.22).

$$(\nu_t + \nu)\partial_z u = \frac{\tau_x^s}{\rho_0} \qquad z = 0 \tag{4.19}$$

$$(\nu_t + \nu)\partial_z v = \frac{\tau_y^s}{\rho_0} \qquad z = 0 \tag{4.20}$$

$$u = 0 \qquad z = -H \tag{4.21}$$

$$v = 0 \qquad z = -H \tag{4.22}$$

The two tracer equations for temperature and salinity have two different surface boundary conditions. The sea surface temperature is dependent on the short-wave radiation (Q_E), latent- (Q_H) and sensible (Q_B) heat flux, which is reflected in the surface boundary condition (equation 4.23). The surface salinity fluxes arising from precipitation and evaporation is neglected, and a zero flux boundary condition is used (equation 4.24). Unfortunately, bottom boundary conditions for the two tracer equations are not explicitly written in the GOTM reports, and must be assumed to be zero, as written in equations 4.25 and 4.26.

$$(\nu_t' + \nu')\partial_z T = \frac{-Q_E - Q_H - Q_B}{C_p \cdot \rho_0} \qquad z = 0 \tag{4.23}$$

$$(\nu_t' + \nu'')\partial_z S = 0 \qquad z = 0 \tag{4.24}$$

$$(\nu_t' + \nu')\partial_z T = 0 \qquad z = -H \tag{4.25}$$

$$(\nu_t' + \nu'')\partial_z S = 0 \qquad z = -H \tag{4.26}$$

The turbulent kinetic energy (k) is assumed to have a zero flux boundary condition, both at surface and bottom (equation 4.27 and 4.29). The dissapation rate, on the other hand, is dependent on the surface or bottom roughness length (z_0) and the distance from the surface or bottom respectively (z). The boundary flux condition is derived from a Direchlet boundary condition and it is the same for surface and bottom, except that the roughness length and distance from boundary is related to the surface or bottom respectively, see equations 4.28 and 4.30).

$$\nu_k \partial_z k = 0 \quad z = 0 \tag{4.27}$$

$$\frac{\nu_t}{\sigma_\epsilon}\partial_z \epsilon = -(c_\mu^0)^3 \frac{\nu_t}{\sigma_\epsilon} \frac{k^{\frac{3}{2}}}{\kappa(z^s + z_o^s)^2} \qquad z = 0 \tag{4.28}$$

$$\nu_k \partial_z k = 0 \quad z = -H \tag{4.29}$$

$$\frac{\nu_t}{\sigma_\epsilon}\partial_z \epsilon = -(c_\mu^0)^3 \frac{\nu_t}{\sigma_\epsilon} \frac{k^{\frac{3}{2}}}{\kappa(z^b + z_o^b)^2} \qquad z = -H \tag{4.30}$$

4.1.5 Calculation of boundary conditions

It was chosen to present the calculation of the boundary conditions in a seperate section, as these calculations are not included in the GOTM documentation. Note that only the surface boundary conditions of momentum (equations 4.19 and 4.20) and the heatflux (equation 4.23) needs to be calculated. The remaining boundary conditions are zero, except for the dissapation rate, which is calculated internally.

The surface stress applied in equation 4.19 and 4.20 is a function of the wind speed and direction. The boundary conditions are calculated according to Bishop (1984), and are presented in equation 4.31 and 4.32. The

ρ_a	ρ_0	c_p	c_t	c_q	q_{10}	L
1.2	1025	4190	0.0010	0.0010	0.005	2447640

Table 4.3: GOTM boundary calculation constants

quadratic drag coefficient is dependent on the wind speed and calculated according to equation 4.33. The input to the GOTM model is the wind stress components (τ).
All constants for calculating the boundary conditions are presented in table 4.3.

$$(\nu_t + \nu)\partial_z u = \frac{\tau_x}{\rho_0} = \frac{\rho_a}{\rho_0} \cdot c_d \cdot |W_{10}| \cdot W_x \tag{4.31}$$

$$(\nu_t + \nu)\partial_z v = \frac{\tau_y}{\rho_0} = \frac{\rho_a}{\rho_0} \cdot c_d \cdot |W_{10}| \cdot W_y \tag{4.32}$$

$$c_d = 7.5 \cdot 10^{-4} + 6.7 \cdot 10^{-5} \cdot |W_{10}| \tag{4.33}$$

$$Q_a = \rho_a \cdot c_p \cdot c_t \cdot |W_{10}| \cdot (T_a - T_w) \tag{4.34}$$

$$E = \rho_a \cdot c_q \cdot |W_{10}| \cdot L \cdot \Big(q_s(T_a) - q_s(T_w)\Big) \tag{4.35}$$

$$q_s(T_w) = \frac{\frac{0.622 \cdot es}{airp}}{1 - \frac{0.378 \cdot es}{airp}} \tag{4.36}$$

$$es = 10^{\frac{0.7859 + 0.03477 \cdot T_w}{1 + 0.00412 \cdot T_W}} \tag{4.37}$$

4.1.6 Initialisation

The initialisation of the current profile is set to zero. This is probably not correct, but no measurements are available, and the error is assumed to be small. Furthermore, the model is expected to approach the correct current profile within a short time period. The period before the current profile

has converged is not important for mixing, as it is typically fully mixed in the winter due to convection, and the biological activity is low, due to the low temperature.

The temperature profile is described analytically, based on an assumed temperature destribution and temperature measurements from two thermistors at 1.5m and 7m depth. A distribution with an upper layer of 3m and a lower layer beginning at 6m depths are assumed. The measured temperature at 1.5m (2.3 degrees) is used to initialise the upper layer, and the bottom layer is initialised to the temperature measured at a depth of 7m (4.3 degrees) The salinity profile is assumed homogenous at 20 ppt and also prescribed analytically.

Both the turbulent kinetic energi (k) and the dissapation rate (ϵ) are set to their respective minimum values described earlier. Certain errors will be expected from this approach, but they are assumed neglectable due to the same factors as are described for the current profile.

4.1.7 Numerical treatment

The GOTM model is run with 15 equally spaced layers to a total depth of 11.5m. The time interval is 20s with output generated every hour. The integration of the equation is handled by the GOTM model.

4.2 The Biological Model

It was decided to develop a model instead of using an existing model, as it was important to clarify the signicant processess in the study area. It is difficult to find an appropriate existing model, as modelling is at a state where models are developed (and calibrated) specifically for local condition, and may not be applied generally. As the local conditions vary much (e.g. lake or ocean, depth, dominating current, temperature) it was not possible to find a model which was developed under the same conditions as the study area in the studied models.

Off course, a model is not developed from scratch, and an effort is made to use well documented formulations of the processess. Pelagic processess are described in section 4.2.1 and sediment processess in section 4.2.2. Forcing and initialisation is described in section 4.2.4 and 4.2.5

4.2.1 Pelagic equations

In contrast with the physical model, which is based on the general GOTM model, the biological model is developed specificly for the study area. Thus, it is necessary to clarify which processesses are considered relevant for the study area and which formulation is used to simulate these processesses.

7 state variables are simulated: 2 types of biota (Phytoplankton and Zooplankton), 2 types of particulate organic matter (dependent on settling velocity), and 3 types of nutrients (phosphorous, nitrate and ammonium). All state variables follow the general one-dimensional equation for tracers (GOTM equation 4.3), here reintroduced as equation 4.38 without the specific molecular diffusivity (ν_t'), which is considered zero except for temperature and salinity. In the following description of processess, only the sources and sinks are presented, however all state variables are subject to turbulent mixing, as in equation 4.38.

$$\partial_t X - \partial_z \nu_t \cdot \partial_z X = R(X) \tag{4.38}$$

Phytoplankton dynamics (equation 4.39) is modelled as growth (μ_p) minus mortality (m_p) and grazing (grz) from zooplankton (e.g. Andersen and Nival (1989)). Phytoplankton growth (equation 4.40) is limited by nutrients, temperature and light (e.g. Andersen and Nival (1989)), mortality

is assumed a constant fraction of the population and grazing is described later.

$$\frac{dPhy}{dt} = \mu_p - m_p \cdot Phy - grz \cdot Zoo \tag{4.39}$$

$$\mu_p = \mu_{max} \cdot Lim_T \cdot Lim_{Par} \cdot min(Lim_N, Lim_P) \cdot Phy \tag{4.40}$$

Temperature limitation (equation 4.41) is modelled by Eppley (1972) according to an exponential law (Q_{10}=2). Photoinhibition (equation 4.42) is modelled according to Platt et al. (1980). The attenuation of light is assumed to follow Lambert-Beer, with a background extinction coefficient and an extinction coefficient related to phytoplankton concentration to include self-shading (equations 4.43 and 4.44).

$$Lim_T = (Q_{10})^{\frac{temp - temp_0}{10}} \tag{4.41}$$

$$Lim_{Par} = \frac{I_z}{k_{par} + I_z} \tag{4.42}$$

$$I_z = PAR_0 \cdot e^{-k_z \cdot z} \tag{4.43}$$

$$k_z = k_{back} + k_{Phy} \cdot Phy \tag{4.44}$$

The nutrient uptake follows the function of Wroblewski (1977), which includes limitation of nitrate uptake at high ammonium concentrations (equation 4.45, 4.46 and 4.47. Phosphorous limitation is modelled by Michaelis-Menten kinetics (equation 4.48). Libieg's minimum law is applied to the limitation of nutrients. Silicium is neglected, as it is only relevant for Diatoms.

$$Lim_N = Lim_{NO_3} + Lim_{NH_4} \tag{4.45}$$

$$Lim_{NO_3} = e^{-\psi \cdot NH_4} \cdot \frac{NO_3}{k_{NO_3} + NO_3} \tag{4.46}$$

$$Lim_{NH_4} = \frac{NH_4}{k_{NH_4} + NH_4} \tag{4.47}$$

$$Lim_p = \frac{P}{k_p + P} \tag{4.48}$$

Zooplankton dynamics is modelled as the difference between assimilated ingested phytoplankton and Zooplankton excretion and mortality (e.g. Andersen and Nival (1989)). Furthermore, they are considered passive, i.e. they are transfered with the turbulent diffusion. The zooplankton formulation is presented in equation 4.49.

$$\frac{dZoo}{dt} = \mu_z - exc_z - m_z \tag{4.49}$$

Growth is modelled as zooplankton ingestion rates (grz, equation 4.51), represented by the Ivlev formulation, modified by Parsons et al. (1967) with constant assimilation (equation 4.50). Excretion (equation 4.52) is assumed to increase exponentially with temperature (Ikeda, 1985) and mortality rate (equation 4.53) is assumed quadratic (Steele and Henderson, 1992).

$$\mu_z = ass \cdot grz \tag{4.50}$$

$$grz = grz_{max} \cdot \left(1 - e^{-iv \cdot (Phy - Phy_{min})}\right) \cdot Zoo \tag{4.51}$$

$$exc_z = exc_0 \cdot (Q_{10_{exc}})^{temp} \tag{4.52}$$

$$m_z = mor_{Zoo} \cdot Zoo^2 \tag{4.53}$$

Ammonium is removed nitrification and uptake by phytoplankton equation 4.47, which prefer ammonium over nitrate (Wroblewski (1977)). Ammonium is generated by remineralisation of particulate organic matter (POM) and excretion by zooplankton. Both nitrification and remineralisation rates are considered constant and the formulation is presented in equation 4.54.

Nitrate is likewise removed by phytoplankton, and regenerated from ammonium at a constant rate. The nitrate formulation is presented in equation 4.55.

$$\frac{dNH_4}{dt} = -\frac{Lim_{NH4}}{Lim_N} \cdot \mu_p - r_{nit} \cdot NH_4 + r_{rem} \cdot POM + exc_z \tag{4.54}$$

$$\frac{dNO_3}{dt} = -\frac{Lim_{NO3}}{Lim_N} \cdot \mu_p + r_{nit} \cdot NH_4 \tag{4.55}$$

The phosphorous equation is very similar to the ammonium equation, except from two points. There is no nitrification to be considered, and everything is divided by the Redfield ratio. For excretion, this assumption migth not hold, e.g. Dolan (1997) investigated phosphorous and ammonia excretion by zooplankton and found N:P-ratios of 2:1 - 8:1. However, since this rate varies significantly from species to species, the Redfield ratio is kept. The phosphorous processess is presented in equation 4.56.

$$\frac{dP}{dt} = \frac{-\mu_p + r_{rem} \cdot POM + exc_z}{N2P} \tag{4.56}$$

It is important to note that the study area apparently changes from phosphorous limitation in the spring and autumn to nitrogen limitation during summer, see section 3.3. However, the model is not able to reproduce this behavior, as a constant N:P-ratio is assumed. As already mentioned, this assumption apparantly does not hold for zooplanktion excretion. Another source of N and P is the sediment release rate (see section 4.2.2), which is not directly related. Finally, the addition of external nutrients from the Lungskile regional treatment plant (see section 2) contributes significant amount of especially nitrogen, however phosphorous load is low. As the contribution from the treatment plant is above the Redfield-ratio (12 $mmol\ N \cdot (mmol\ P)^{-1}$), this input would cause P-limitation, so it can not explain the change from P- to N-limitation.

Since the model at present does not include any of these processess, the model can not be expected to reproduce the observed nutrient concentrations and these can not be used for validation.

The 2 POM types reflects slow settling (dead phytoplankton) and rapidly settling (zooplankton and unassimilated ingested phytoplankton) material. These contributions to POM has been previously described. Both types are assumed to be remineralised at a constant rate, consistent with other models (e.g. Andersen and Nival (1989)). POM settling out of the bottom box enters the sediment, see section 4.2.2 and 4.2.3. The dynamics for the two POM types are presented in equation 4.57 and 4.58.

$$\frac{dPOM_P}{dt} = m_p \cdot Phy - r_{rem} \cdot POM_P - W_{POM_P} \cdot \partial_z POM_P \quad (4.57)$$

$$\frac{dPOM_Z}{dt} = \frac{1-ass}{ass} \cdot grz + mor_z - r_{rem} \cdot POM_Z - W_{POM_Z} \cdot \partial_z POM_Z \quad (4.58)$$

4.2.2 Sediment equations

The choice of a sediment model is based largely on the work of Soetart et al. (2000), which provides a framework for analysis. They classify sediment models in 4 levels of increasing complexity, and they reserve a level 0 for the case of no sediment model. In fact, many of the studied models (Everbecq et al. (2001), Skliris et al. (2001), Oguz et al. (1999), Chifflet et al. (2001)) was ignoring the sediment (level 0). The level are described in table 4.5.

Following the recommandations of Soetart et al. (2000) a vertically integrated (level 3) model was chosen to conserve mass and minimise computations. The model is simplified by considering all POM easily degradable and all degraded POM is turned into nitrate and phosphorous, which is immidiately release to the bottom pelagic layer. All organic sediment matter is assumed mineralised within a year, so the initial concentration is set to zero.

The formulation for the sediment box is shown in equation 4.59.

$$\frac{dSed}{dt} = W_{POM} \cdot \partial_z POM_P + W_{POM} \cdot \partial_z POM_Z - r_{rem} \cdot Sed \quad (4.59)$$

Other, more complex, models were considered (Soetart et al. (2001) and Baretta et al. (1995)), but the vertically integrated model was preferred because of its low demand on initialisation.

Constant	Description	Value	Unit
μ_{max}	Maximum phytoplankton growth	1.5	day^{-1}
m_p	Phytoplankton mortality	0.05	–
Q_{10}	Temperature coefficient for phytoplankton	2	–
$temp_0$	Reference temperature	10	C
k_{par}	Solar radiation limitation coefficient	100	W
k_{back}	Background extinction coefficient	0.35	m^{-1}
k_{phy}	Phytoplankton extinction coefficient	0.05	$m^{-1} \cdot (mmol\ N \cdot m$
k_{NO_3}	Nitrate limitation half coefficient	1	$mmol\ N \cdot m^{-3}$
k_{NH_4}	Ammonium limitation half coefficient	0.7	$mmol\ N \cdot m^{-3}$
ψ	Nitrate inhibition from ammonium	1.5	$(mmol\ N \cdot m^{-3})^{-1}$
k_p	Phosphorous limitation half coefficient	0.1	$mmol\ P \cdot m^{-3}$
$N2P$	Nitrate to phosphorous ratio	16	$mmol\ N \cdot (mmol\ F$
ass	Assimilatino constant	0.8	–
iv	Ivlev coefficient for grazing	0.5	$mmol\ N \cdot m\ -3$
Phy_{min}	Grazing treshold	0.2	$mmol\ N \cdot m^{-3}$
exc_0	Excretion at 0 degress	0.3	–
$Q_{10_{exc}}$	Temperature coefficient for excretion	1.025	–
mor_{Zoo}	Zooplankton quadratic mortality	0.1	–
W_{POM_P}	Settling velocity for phytoplankton POM	0.5	$m \cdot m^{-1}$
W_{POM_Z}	Settling velocity for phytoplankton POM	10	$m \cdot m^{-1}$
r_{rem}	POM remineralisation rate	0.1	–
r_{nit}	Nitrification rate	0.1	–

Table 4.4: Biological constants

Level	Description
level 4	Dynamic, vertically resolved biogeochemical model
level 3	Dynamic vertically integreted model
level 2	Reflective type boundary
level 1	Exchange or bottom water imposed
(level 0)	Sediment ignored

Table 4.5: Sediment model levels

4.2.3 Boundary conditions

The biological varibles (phytoplankton and zooplankton) has a no-flux boundary condition, i.e. no phytoplankton or zooplankton enters or leaves the area. Thus, e.g. exchange with Havstenfjorden is ignored.

The boundary conditions for nutrients arise from the coupling to the sediment. Phosphorous and nitrogen enters the bottom box at a rate prescribed by equation 4.59. Exchange with Havstensfjorden is ignored, as for the biological variables. Furthermore, input from the regional treatment plant in Lungskile (see section 2) is not included, as it does not explain the alternation between P- and N-limitation.

For POM, no horisontal fluxes are considered, and the vertical boundary condition is the settling out of the bottom box.

4.2.4 Forcing

The biological model is forced by solar radiation, temperature and turbulent mixing (modelled by the eddy diffusivity coefficient). The first forcing function is measured from a nearby weather station and converted to photoactive radiation (PAR) assuming 40% of all radiation lies within that range, see figure rad. The latter two forcing functions are calculated by the physical model (see section 4.1) and used to force the model. The annual radiation can be viewed in figure 1 in chapter 2, the temperature development and daily eddy diffusivity are presented in the result section of the physical model, figure 10 and 11.

State variable	1.5m	7m
Phy	1	1
Zoo	0.4	0.4
P	0.6	0.6
NO_3	12.02	9.88
NH_4	0	0
POM	0	0

Table 4.6: Initial values for biological state variables

4.2.5 Initialisation

The initial values for the state variables are presented in table 4.6. Phytoplankton is initialised to the winter values measured in Havstensfjorden, and zooplankton is initialised to a value, that ensures survival until the spring bloom. Both phosphorous and nitrate is initialised to the highest measured values in Lungskile. Since the biological activity is low in the winter, ammonium and the 2 POM pools are assumed zero.

4.3 The Mussel Model

4.3.1 Choice of model

Several formulations for mussel dynamics was studied (e.g. Dowd (1997), Campbell and Newell (1998), Grant and Bacher (1998)) before a model by Lamy et al. (2000) was selected. The choice of this model was based on their detailed description of mussel ingestion. In fact, the model by Lamy et al. (2000) was the only one to include a saturation response due to maximum ingestion. As the purpose of this model is to simulate mussel growth in different phytoplankton concentrations, the saturation response was considered important to include. Furthermore, the model also includes pseudofaces production at high filtration rates and a selection of phytoplankton over detritus. All this combined renders the model by Lamy et al. (2000) the most appropriate.

The model does not aim to reproduce measurements, but a merely provided for comparison between different depth. Thus, the model will not be validated or calibrated.

4.3.2 Equations

In this section, the equations for the mussel model is presented. The equation are based on Lamy et al. (2000). Please refer to table 4.7 for explanations and values for constants.

The mussel dynamics is described by a mass balance comprised of assimilated material and respiration (equation 4.60).

$$\frac{dMus}{dt} = Mus_{Ass} - Mus_{Res} \tag{4.60}$$

The assimilated material is consists of phytoplankton (Phy) and detritus (Det). Phytoplankton is easier to assimilate, which is reflected in different assimilation coefficients (equation 4.61). The assimilation is determined from the time in the gut (Gut_{RT}) and a coefficient for how long time it takes for 50% of the ingested mass to be assimilated (equation 4.62 and 4.63). The higher time for assimilation of detritus (see constants in table

4.7) simulates the slower assimilation. The time in the gut is defined as the gut volume divided by the ingested mass, consistent with retention time calculation (equation 4.64).

$$Mus_{Ass} = Ass_{Phy} \cdot Ing_{Phy} + Ass_{Det} \cdot Ing_{Det} \tag{4.61}$$

$$Ass_{Phy} = \frac{gut_{RT}}{gut_{RT} + K_{Ass_{Phy}}} \tag{4.62}$$

$$Ass_{Det} = \frac{gut_{RT}}{gut_{RT} + K_{Ass_{Det}}} \tag{4.63}$$

$$gut_{RT} = \frac{gut_{Vol}}{Ing_{SPM}} \tag{4.64}$$

The ingested mass (Ing_{Phy} and Ing_{Det}) is dependent on a clearance rate (Cle), the filtrated concentrations ($Filt_{Phy}$ and $Filt_{Det}$) and coefficient for rejection (rej) and selection (sel). The filtration is shown in equation 4.65 and 4.66, and ingestion is presented in equation 4.67 and4.68.

$$Filt_{Phy} = Cle \cdot Phy \tag{4.65}$$

$$Filt_{Det} = Cle \cdot Det \tag{4.66}$$

$$Ing_{Phy} = Filt_{Phy} \cdot (1 - rej \cdot sel) \tag{4.67}$$

$$Ing_{Det} = Filt_{Det} \cdot (1 - rej) \tag{4.68}$$

The clearance rate (Cle) is limited by one of two possible maximum rates. Either, a maximum clearance rate, if concentrations are low, or a maximum ingestion rate. If the maximum ingestion rate is reaches, clearance is calculated to match the maximum ingestion (equation 4.69). The ingested suspended paticulate matter (SPM) includes inorganic matter as silt (equation 4.70). The model is developed in a highly turbid area in the Netherlands and silt is not present in significant concentrations in the

study area. The equations are here presented including silt (equation 4.71 and 4.72) to keep the original equations from the reference, but the silt concentration is assumed zero.

$$Cle = Cle_{Max} \cdot min\left(1, \frac{Ing_{Max}}{Ing_{SPM}}\right) \tag{4.69}$$

$$Ing_{SPM} = Ing_{Silt} + GrC \cdot (Ing_{Phy} + Ing_{Det}) \tag{4.70}$$

$$Filt_{Silt} = Cle \cdot Silt \tag{4.71}$$

$$Ing_{Silt} = Filt_{Silt} \cdot (1 - rej) \tag{4.72}$$

Finally, the rejection (rej) and selection (sel) needs to be defined. The rejection accounts for pseudofaces production when the filtration (equation 4.74) reaches a treshold level ($Filt_{Th}$). This prevents overloading of the gut, when the filtration is high. The selection coefficient models the mussels ability to select a good food source (e.g. phytoplankton) over detritus and silt. The formulation of rejection and selection is presented in equation 4.73 and 4.75.

$$Rej = max\left(0, Rej_{Max} \cdot \frac{Filt_{SPM} - Filt_{Th}}{Filt_{SPM} - Filt_{Th} + K_{Rej}}\right) \tag{4.73}$$

$$Filt_{SPM} = Filt_{Silt} + GrC \cdot (Filt_{Phy} + Filt_{Det}) \tag{4.74}$$

$$Sel = 1 - Sel_{Max} \cdot \frac{Rej \cdot Filt_{SPM}}{Rej \cdot Filt_{SPM} + K_{Sel}} \tag{4.75}$$

The assimilation (Mus_{Ass}) from equation 4.60 has now been described, but the respiration ($Muss_{Res}$) still needs to be adressed. A constant basal respiration (Res_{Ba}) and an active respiration related to assimilation is considered. The formulation for respiration is shown in equation 4.76.

$$Mus_{Res} = Res_{Ba} + Ass_{Cost} \cdot Mus_{Ass} \tag{4.76}$$

Symbol	Description	Value	Unit
GrC	mol C to g DW ratio	30	$g\ DW(mol\ C)^{-1}$
Ing_{Max}	Maximum ingestion rate	$7.9 \cdot 10^{-3}$	$g\ DW \cdot h^{-1} \cdot ind^{-1}$
Rej_{Max}	Maximum rejection rate	0.97	-
$Filt_{Th}$	Treshold for pseudofaces	$7.8 \cdot 10^{-3}$	$g\ DW \cdot h^{-1} \cdot ind^{-1}$
K_{Rej}	Coefficient for rejection	$9.4 \cdot 10^{-3}$	$g\ DW \cdot h^{-1} \cdot ind^{-1}$
Sel_{Max}	Maximum selection coefficient	0.7	-
K_{Sel}	Coefficient for selection	0.01	$g\ DW \cdot h^{-1} \cdot ind^{-1}$
$K_{Ass_{Phy}}$	Coefficient for algae assimilation	0.5	h
$K_{Ass_{Det}}$	Coefficient for detritus assimilation	5	h
Gut_{Vol}	Gut volume	0.01	$g\ DW \cdot ind^{-1}$
Res_{Ba}	Basal respiration	$1.3 \cdot 10^{-4}$	$mol\ C \cdot d^{-1} \cdot ind^{-1}$
Ass_{Cost}	Fraction of assimilation respired	0.04	-

Table 4.7: Constant for the mussel model

Chapter 5

Results and discussion

5.1 The Physical Model

5.1.1 Temperature

Figure 5.1 shows the simulated temperature profile calculated by the GOTM model. A thermocline starts to build up at the 8th of April, where temperature difference between 1.5m and 7m exceeds 1 degree for the first time. This stratification remains until the 26rd of May, when the water column is mixed by a strong wind event (See figure 3.8). The storm event fully mixes the water column, which is also reflected in the observations (figure 3). The temperature reaches a maximum of 25. In Autumn, the radiation is no longer strong enough to build up a new thermocline, and the Autumn storms keeps the water column well mixed. The water column temperature remains more or less uniform in the rest of the year, with temperature differences of less than 1 degree.

Temperature is measured at 2 depth (1.5m and 7m depth) from Nov 30 1999 to Nov 30 2000 at 30 minutes intervals by thermistors. The measurements are presented in figure 5.2 as a solid line, and the simulated temperature is shown as a dotted line. During the gradual heating of the water column before stratification, the simulated temperature is too high. The timing of the thermocline, measured as the date where the temperature difference between 1.5 and 7m depth increases to more than 1 degree, is the 8th

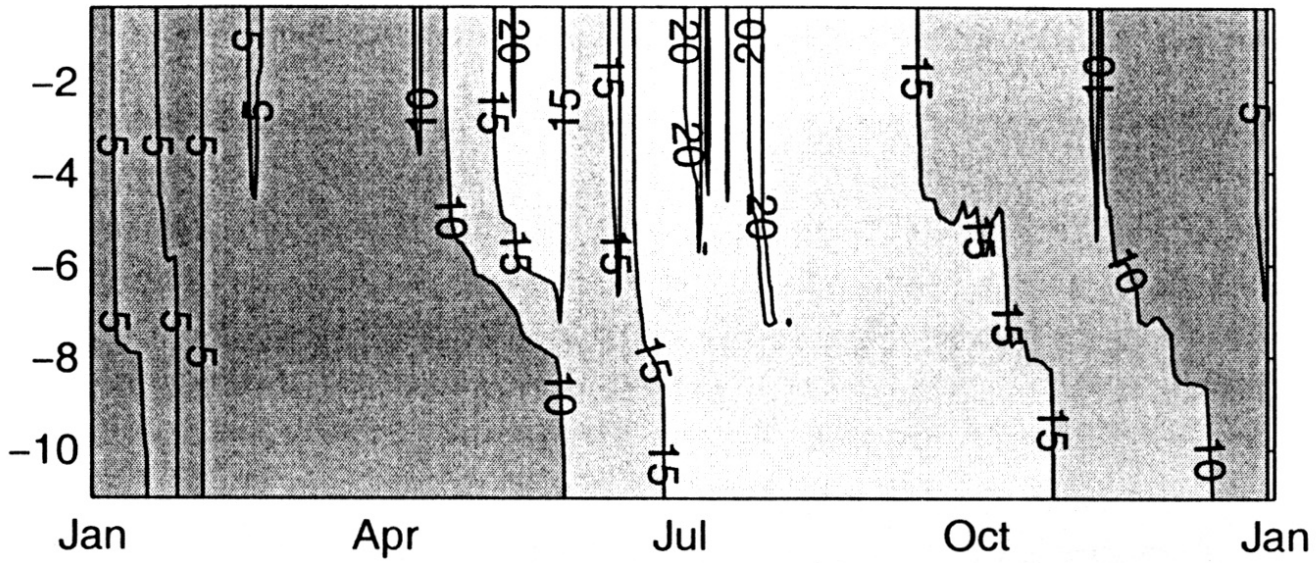

Figure 5.1: Simulated temperature

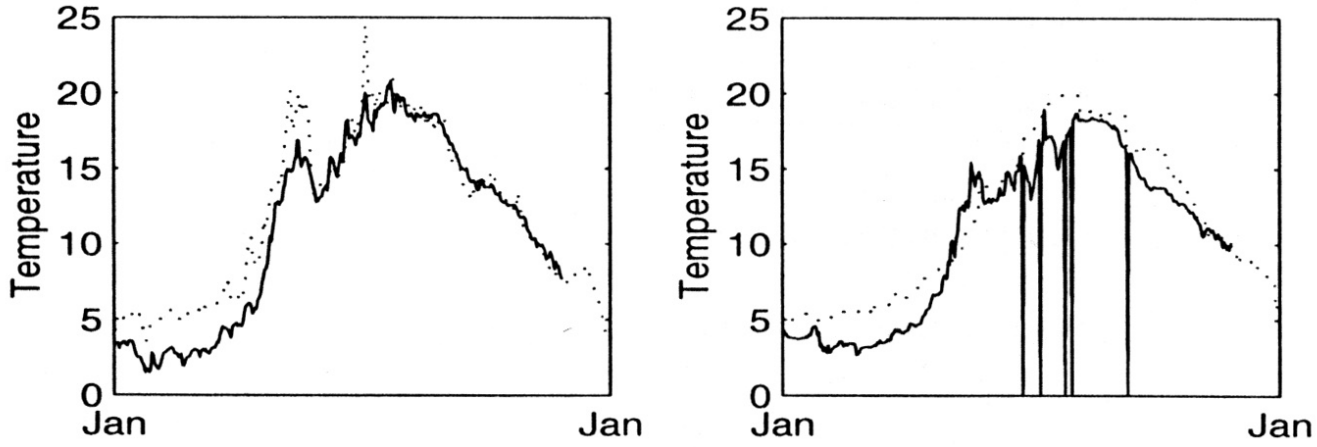

Figure 5.2: Simulated and observed temperature

of April calculated for both measured and simulated values. The effect of the storm on the 26rd of May is visual both in the observations and the simulations, the temperature change at both depths indicative of full mixing. Autumn values are generally well represented, both simulation and observation showing temperature differences between top and bottom temperature of less than 1 degree.

5.1.2 Mixing

As an indication of the turbulent mixing, the Mixed Layer Depth (MLD), calculated as the depth where the Turbulent kinetic energy declines below

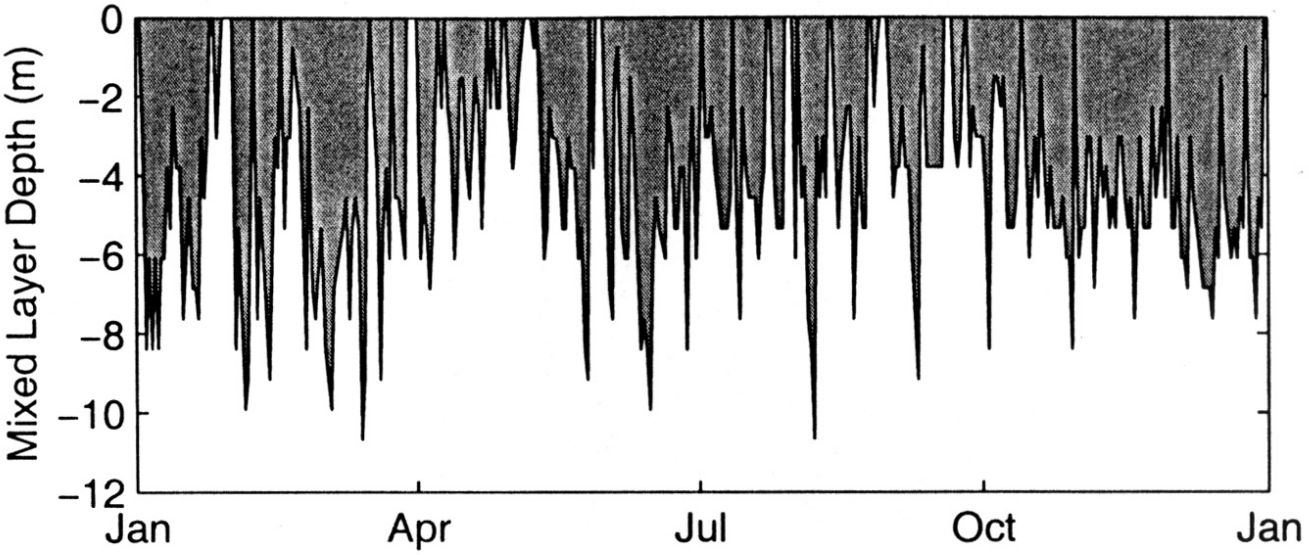

Figure 5.3: Simulated mean daily mixed layer depth (calculated from the criteria $tke < 10^{-5}$)

$5 \cdot 10^{-5}$ m^2/s^2, is chosen. The calculated daily mean MLD is shown in figure 5.3.

The water column is generally well mixed until the beginning of April, where the MLD starts to increase. It is followed by a period of approximately 3 weeks with low windspeed (see figure 3.8), with leads to a shallow MLD. A strong wind event on the 26rd of May fully mixes the water column, and it is fully mixed several times in the next week. During Autumn the water column is generally well mixed.

5.1.3 Sensitivity to salinity

As already meantioned in section 4.1.3 GOTM does not include any sources or sinks of the salt concentration (see equation 4.25 and 4.27). However, a salinity gradient causes a density gradient, which generates bouyancy production (see equations 4.10 and 4.11). Increased boyancy production stabilises the water column and inhibits mixing. Without any sources or sinks of salt, the salinity concentration remains uniform after a complete mixing event. After such an event, mixing would be overestimated.

To investigate this, CTD profiles of salt obtained during a campaign from the 10th to the 20th of July 2000 is used to simulated Mixed Layer Depth. The model was run both without relaxation and with a relaxation time of

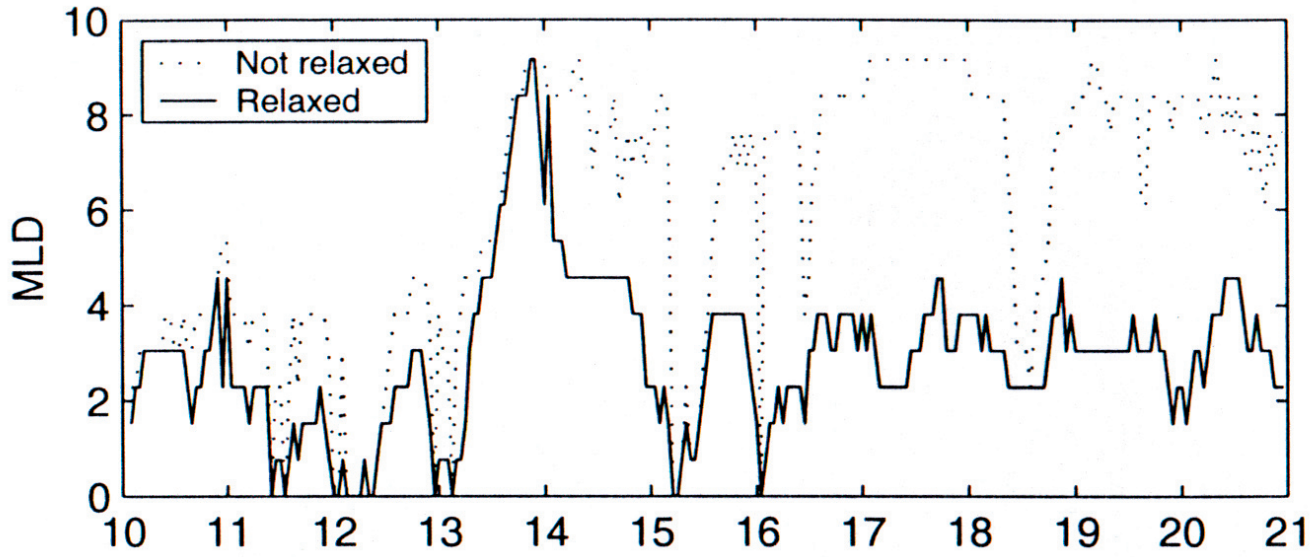

Figure 5.4: Sensitivity to salinity relaxed to observed values

3 hours to the observed salinity profiles, see figure 5.4. The case without relaxation corresponds to the standard setup of the GOTM model.

This sensitivity analysis clearly shows the significance of local salinity profiles. The approximation of using monthly measurements from Galterö is significantly better than using no salinity profiles, but the mixing will presumably be more in accordance with Galterö conditions than local Lungskile mixing. This limitation could introduces differences between the mixed layer depth encountered during sampling of biological variables, which should be taken into account when evaluating these results.

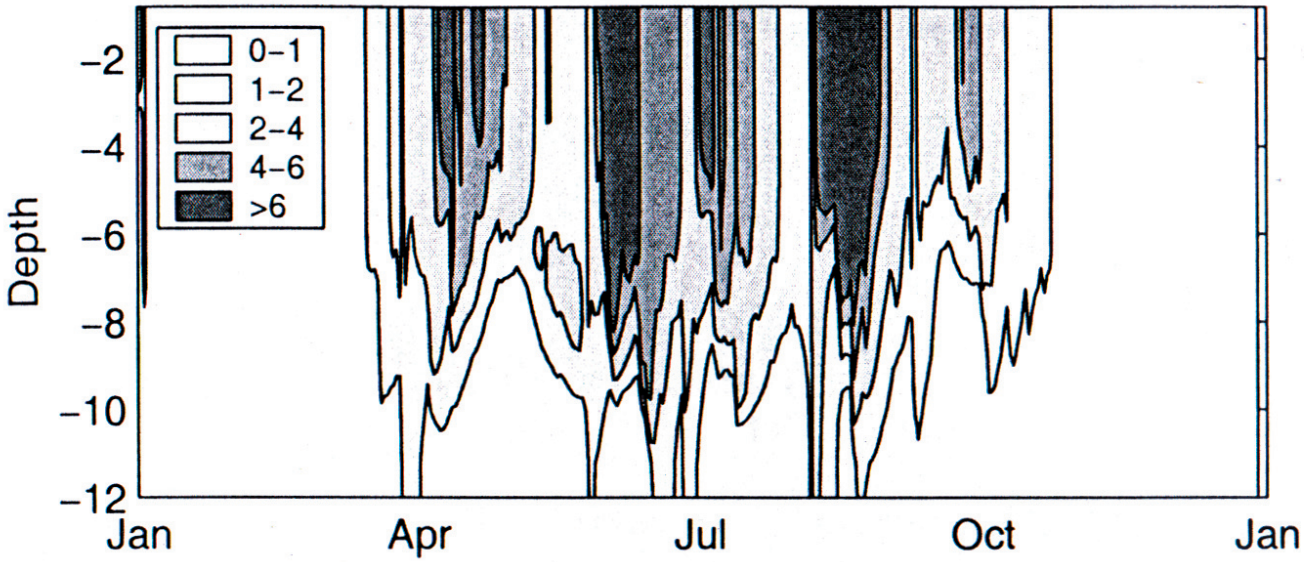

Figure 5.5: Simulated Chla a concentration

5.2 The Biological Model

5.2.1 Phytoplankton

The simulated spring bloom begins in March, consistent with observations (see section 3.4). After April, nutrients are limiting, causing a decline in chl a due to natural mortality and zooplankton grazing. The wind event on the 27th of May mixes the water column thouroughly, bringing remineralised nutrients from the sediments to the surface. This initialised a second bloom, where high chl a values are found in the entire water column. This cycle is repeated twice again between July and October. Organic material settles to the bottom, in practice removing it from the phytoplankton population, which declines until a new wind event once again replenishes surface waters. The two last bloom is however significantly lower in the depth. After the last bloom, the solar radiation and temperature declines and phytoplankton slowly reaches winter levels. The simulation phytoplankton concentration are shown in figure 5.5.

Figure 5.6 compares observed and simulated concentrations. Measurements during the campaign from the 10th to the 20th of July 2000 is not included, as the model aims to reproduce annual values, and is not expected to simulate daily variations.

The model simulates the observations reasonably well at 1.5m depth. The model predicts a spring bloom, which is not caugth by the sampling dates,

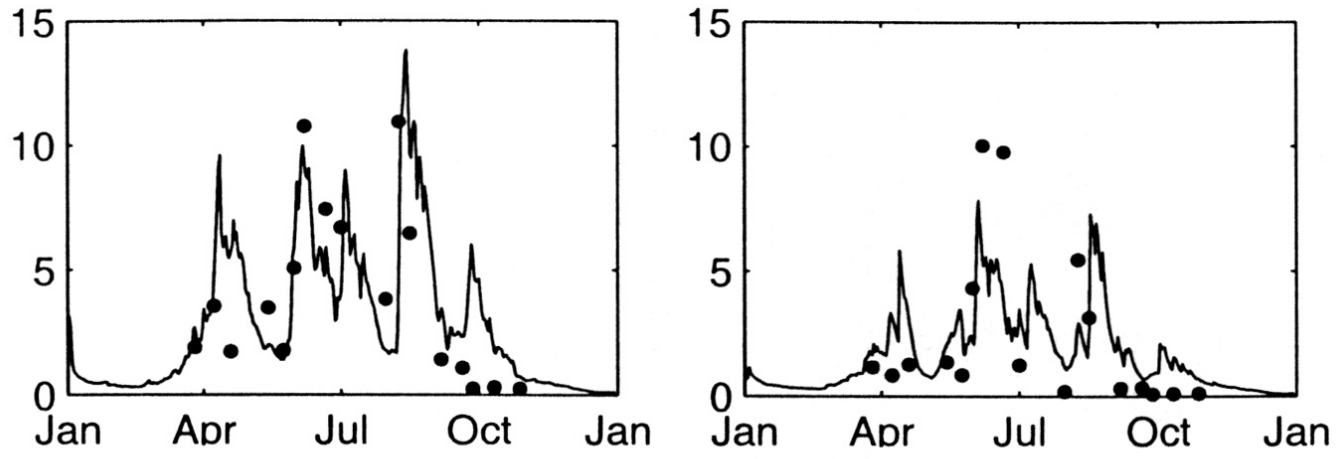

Figure 5.6: Simulated and observed Chl a concentrations [Left panel: 1.5m Right panel: 7m]

and the high concentration on the 9th of April is not consistent with observations. The rapid phytoplankton growth between the 1st and the 10th of June is well modelled and both the timing and the magnitude of the bloom is in accordance with observation. The summer values after the 10th of June is at a level which the observations supports. The concentration is too low before the peak in August, but the observed rapid increase is simulated and the magnitude is in the range of the observations. The model is not able to reproduce the low observations in September/October, but as already mentioned in section 3.4 they are lower than winter values for the area. Furthermore, observations show no indication of limiting nutrients or ligth, and there is no apparent reason for increased grazing. However, the mussel long-line systems in Lungskile constitutes a sink of phytoplankton, and that migth be significant.

The observations are generally low at 7m depth, except from the period from the 1st to the 10th of June, where observations indicated a deep bloom. The model simulates the general low values, but the magnitude of the bloom in June is significantly low at 7m depth. This is probably caused by an underestimation of the mixed layer depth during the two blooms, which would mix surface phytoplankton deeper into the water column.

As pointed out in section 5.1.3, the physical model is very sensitive to salinity profiles, which are not measured for the study area. The limitation from approximating salinity profiles with monthly measurements from Galterö would therefore impact the simulation of the blooms at 7m depth.

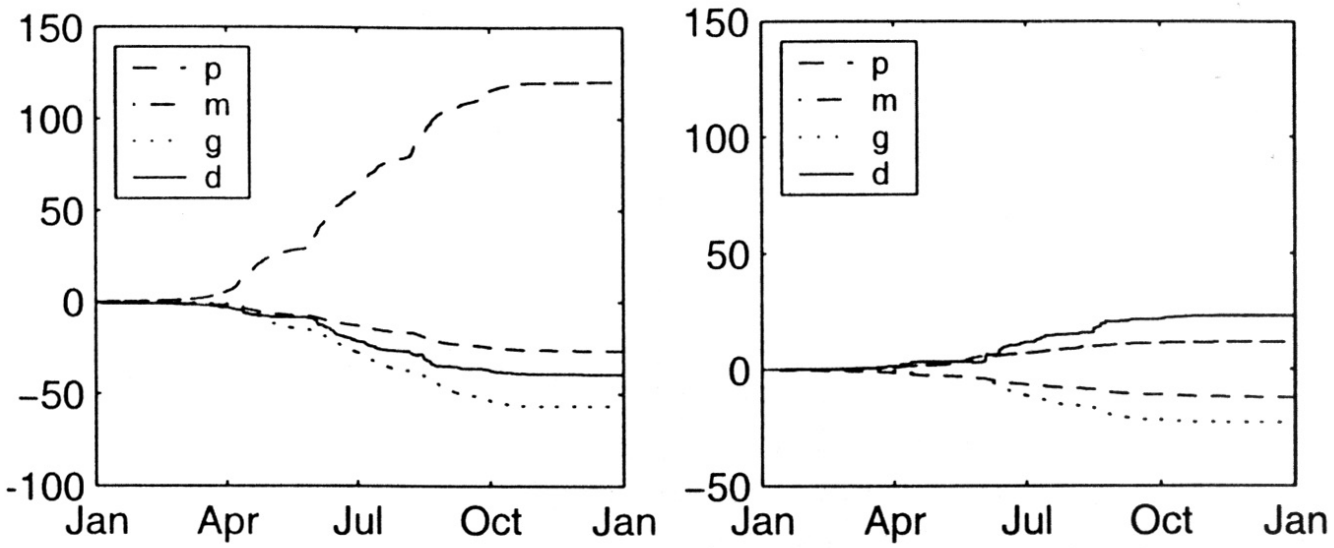

Figure 5.7: Integrated phytoplankton processes [Left panel: 1.5m Right panel: 7m; p=Primary production m=Mortality g=Grazing d=turbulent diffusion]

5.2.2 Phytoplankton processes

Figure 5.7 shows the integrated product of the 4 phytoplankton processess (see equation 4.39) at 1.5m and 7m depth. There is a marked shift in the composition of the magnitude of the processes. At 1.5m depth, photosynthesis is the dominating process, but approximately 1/3 of the production is transfer to another depth by turbulent diffusion. On the contrary, turbulent diffusion contributes more to the phytoplankton concentration at 7m depth than phytosynthesis does. The decrease of photosynthesis with depth is expected from the attenuation of ligth and shading from other phytoplankton (see equations 4.43 and 4.44), if impact from nutrients are ignored. However, the transfer of phytoplankton by mixing to the lower layers decreases the differences due to primary production and illustrates how important turbulent mixing is. Furthermore, lower loss rates at 7m depth compared to 1.5m depth also contributes to diminish the effect of higher production nearer to the surface.

Several authors (e.g. Skliris et al. (2001)) have studied the importance of wind mixing. Most studies have concerned deep areas, but wind mixing migth have an even bigger impact in shallow areas. In the current model, turbulent mixing constitutes a large contribution to subsurface phytoplankton concentration. Compared to Skliris et al. (2001) and Wroblewski (1977), who both found that the bloom begins after relaxation of

Process	Magnitude (mmol N)
Photosynthesis	568
Phytoplankton mortality	192
Zooplankton grazing	383
Zooplankton mortality	146
Zooplankton excretion	165
Zooplankton POM remineralisation	19
Phytoplankton POM remineralisation	145
Zooplankton POM settling	271
Phytoplankton POM settling	62
Released from sediment	333

Table 5.1: Mass balance between processess

the wind, the bloom in this shallower water column initiates during the wind event. This results in a mixing of the high surface phytoplankton concentration to deeper levels, an effect which was not seen in any of the two studies at deep water.

5.2.3 Mass balance

Table 5.1 shows the total transfer between state variables due to different processess. Of the 568 mmol N incoorperated in via photosynthesis into phytoplankton biomass, 2/3 are lost to grazing and 1/3 to natural mortality. Zooplankton losses is split almost evenly in excretion and mortality. 192 mmol N is tranfered to phytoplankton POM and 223 mmol N is converted into zooplankton POM, 77 of which is unassimilated grazed phytoplankton. However, most (75%) of the phytoplankton POM is remineralised, whereas for zooplankton POM, most settles to the sediment. All sedimented material is released again within the year.

The mass balance shows the importance of settling, as 59% of primary production settles to the sediment before being released again as dissolved nutrients. Compared to studies of replenishment of nutrients from deep areas, the sediment constitutes a big difference. In deep areas, the wind mixing erodes the nitricline (e.g. Skliris et al. (2001)), which requires the wind to mix even deeper the next time to replenish the surface nutrients.

However for shallow areas as Lungskile, the sediment constitutes a lower boundary where nutrients are present. Thus, every time the mixed layer depth is equal to the height of the water column, nutrients are supplied to the surface. The makes shallow areas potentially more productive, as nutrients are not as readily lost (or inaccessible) as in deeper areas.

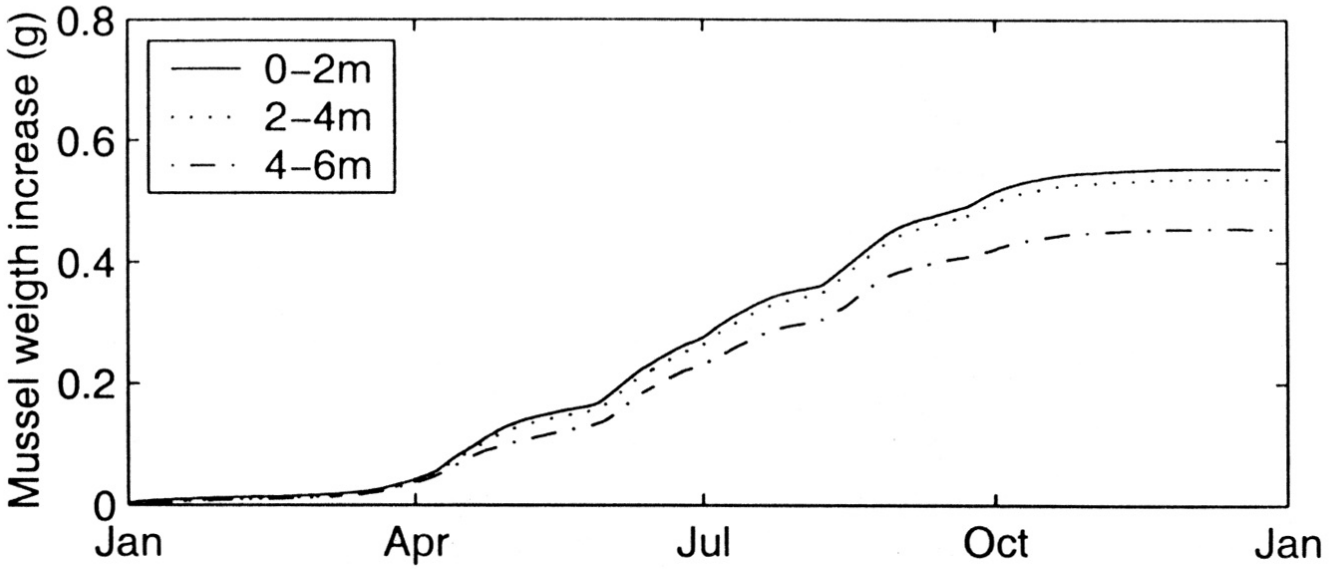

Figure 5.8: Simulated weight gain for an individual mussel in 3 depths

5.3 The Mussel Model

This section is studying the impact of phytoplankton concentration on mussel ingestion at two levels: A simple analytic calculation and a detailed mussel ingestion model. The analytical solution is presented to evaluate the impact without introducing the possible errors of model parameters. In fact, the analytical is only based on a maximum ingestion level for mussel and the chl a to carbon ratio. The detailed model describes assimilation of seston (phytoplankton, particulate organic matter and silt) in more detail, e.g. the quality of the food source is included. As previously stated in section 4.3.1, it is in no way an attempt to present a fully calibrated, validated model based on the mussel samples, but merely to highlight differences in growth due to the simulated chl a concentrations.

5.3.1 Mussel weight gain

Figure 5.8 shows the simulated weight increase of an individual mussel exposed to a phytoplankton concentration equal to the profiles simulated by the biological model. The figure presents an average weight gain for 3 depths, consistent with the analyzed depth in section 3.1. The results does not include differences in in food quality (POM concentration is set to zero), but only differences in phytoplankton concentration.

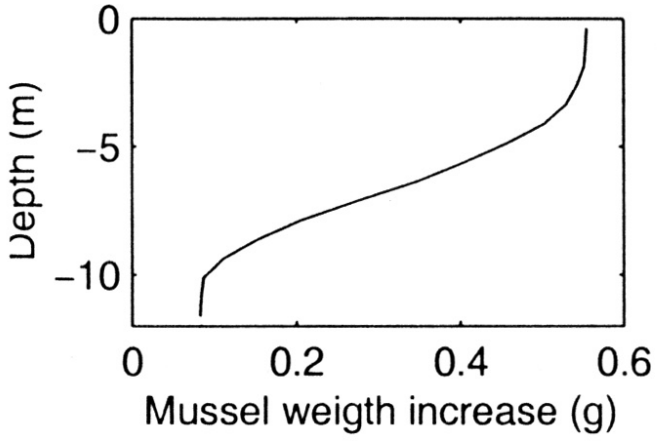

Figure 5.9: Simulated weight gain for an individual mussel as a function of depth

The results clearly show that there is only limited difference in weight gain between 0-2m and 2-4m; however, the weight gain at 4-6m is significantly lower. As already noted in section 5.2.1, the simulated blooms are underestimated at 7m depth compared to observations. A major part of the weight gain occurs during these blooms, and if more food were available for mussel at 4-6m depth during these periods, the difference in weight increase would be smaller.

The simulated values for weight gain during a year are 0.55, 0.53 and 0.45 g for 0-2m, 2-4m and 4-6m respectively. Thus, the difference between 0-2m and 2-4m is only 3.6%, comparable to analysis of the mussel samples in section 3.1. The mussels gain 17,8% and 22,2% more at the top 4 meters compared to below, significantly more than estimated in section 3.1. Again, note that this effect is expected to be smaller.

5.3.2 Depth dependency

Figure 5.9 shows the simulated weight gain for an individual mussel during one year. There is a clear decrease in gain after 4m depths. As already argued, this threshold of no decrease might be lower in reality, if phytoplankton is underestimated in depth.

The figure also illustrates the importance of mathematical modeling as a management tool. The model can aid in deciding the depth of the mussel culture. If the manager knows that he can only sell mussels, which has gained 0.3 g during a year, the model will suggest a depth of 7m.

Chapter 6

Conclusion

This report proposes mathematical modeling as a management tool in mussel production. The aim was to explain differences in growth and to evaluate the use of mathematical models as a design tool.

The model is apparently able to explain the observed low vertical differences in growth. According to the model, the low depth (12m) in the study area provides suitable conditions for regular nutrient pulses of regenerated nutrients from the sediment. During wind events, new phytoplankton growth is stimulated when nutrients are replenished from the lower layer due to mixing. Concurrently, high surface phytoplankton concentrations are mixed deep into the water column, presumably creating uniform concentration throughout the mussel culture. As a significant part of the mussel weight gain occurs during blooms, this might explain the low vertical differences in mussel growth within the long-line culture. This thesis is also supported by observations with more or less equal concentrations at 1.5m and 7m depth during blooms.

The model is also considered valuable as a management tool. Design parameters, e.g. depth of the mussel culture, can be defined from design criterions, e.g. minimum annual weight gain. However, for the model to become a practical tool, it is necessary to improve the model on several points: a) to conduct regular measurements of salinity profiles to support the physical model, b) to quantify sediment in situ release rates (e.g. by sediment incubations) to improve the sediment model and c) to determine the factors controlling the switch from P- to N-limitation during the year.

However, this model should only be considered a first tentative step towards a practical tool, and perhaps this report will bring interest in continuing the iterative cycle of modeling and experiments. If so, I hope the model will be able to direct the next step.

Bibliography

V Andersen and P Nival. Modeling of phytoplankton population-dynamics in an enclosed water column. *Journal of the marine biological association of the united kingdom*, 69(3):625–646, August 1989.

J.W. Baretta, W. Ebenhöh, and P Ruardij. The european regional seas ecosystem model, a complex marine ecosystem model. *Netherlands Journal of Sea Research*, 33(3/4):233–246, 1995.

H.A. Beadman, R.I. Willows, and M.J. Kaiser. Potential applications of mussel modeling. *Helgoland Marine Research*, 56:76–85, 2002.

Joseph M. Bishop. *Applied ocaonography.* Wiley, 1984.

G Björk, O Liungman, and L Rydberg. Net circulation and salinity variations in an open-ended Swedish Fjord System. *Estuaries*, 23(3):367–380, June 2000.

Hans Burchard, Karsten Bolding, and Manuel R. Villarreal. GOTM - a General Turbulence Model. *Journal of Marine Systems*, 26:259–288, 2000.

Hans Burchard and Ole Petersen. Models of turbulence in the marine environment - a comparative study of two-equation turbulence models. *Journal of Marine Systems*, 21:29–53, 1999.

Daniel E. Campbell and Carter R. Newell. MUSMOD, a production model for bottom culture of the blu mussel, Mytilus edulis L. *Journal of Experimental Marine Biology and Ecology*, 219:171–203, 1998.

Fa Chen and J.D. Annan. The influence of different turbulence schemes on modelling primary production in a 1D coupled physical-biological model. *Journal of Marine Systems*, 26:259–288, 2000.

Marina Chifflet, Valerie Andersen, Louis Prieur, and Ivan Dekeyser. One-dimensional model of short-term dynamics of the pelagic ecosystem in the NW Mediterranean Sea: effects of wind events. *Journal of Marine Systems*, 30:89–114, 2001.

J.R. Dolan. Phosphorous and ammonia excretion by planktonic protists. *Marine Geology*, 139:109–122, 1997.

Michael Dowd. On predicting the growth of cultured bivalves. *Ecological modelling*, 104:113–131, 1997.

Lars Edler. *Växtplankton rapport för 2000.* SMHI (Swedish Meteorological and Hydraulic Institute), 2000.

RW Eppley. Temperature and phytoplankton growth in sea. *Fishery bulletin*, 70(4):1063–1085, 1972.

E. Everbecq, V. Gosselain, L. Viroux, and J.-P. Descy. Potamon: A dynamic model for predicting phytoplankton composition and bomass in lowland rivers. *Wat. Res.*, 35(4):901–912, 2001.

Elizabeth Gosling, editor. *The mussel mytilus: ecology, physiology, genetics and culture.* Elsevier, 1992.

J. Grant and C. Bacher. Comparative models of mussel bioenergetics and their validation at field culture sites. *Journal of Experimental Marine Biology and Ecology*, 219(1-2):21–44, 1998.

T Ikeda. Metabolic rates of epipelagic marine zooplankton as a function of body-mass and temperature. *Marine biology*, 85(1):1–11, 1985.

Cato Ingemar. *Sedimentological investigations of the Boguscoast 1995 and recent trends in coastal environmental sediment quality - a report from 5 trend-monitoring programs.* Elanders Gotab, Stockholm, 1997.

François Lamy, Peter M.J. Herman, Hans Burchard, Johannes de Clippele, Anja S. Hansen, Jacco Kromkamp, Flemming Møhlenberg, Jens K. Petersen, and Theo C. Prins. A coupled physical-biological model to study the spatial distribution of mussels in the Oosterschelde - Part 1. *Submitted*, 2000.

Lann and Oscarson. *Hur man mindskar kvä vetilforsel.* ?, 2000.

HC Nilsson and R Rosenberg. Benthic habitat quality assessment of an oxygen stressed fjord by surface and sediment profile images. *Journal of marine systems*, 11(3-4):249–264, June 1997.

Temel Oguz, Hugh W. Ducklow, Paola Malanotte-Rizzoli, James W. Murray, E.A. Shushkina, V.I. Vedernikov, and Umit Unluata. A physical-biochemical model og plankton productivity and nitrogen cycling in the Black Sea. *Deep-Sea Research I*, 46:597–636, 1999.

T.R. Parsons, R.J. Lebrasseur, and J.D. Fulton. Some observations on the dependence of zooplankton grazing on cell size and concentration of phytoplankton blooms. *J. Oceanogr. Soc. Jpn.*, 23:10–17, 1967.

T Platt, CL Gallegos, and WG Harrison. Photoinhibition of photosynthesis in natural assemblages of marine-phytoplankton. *Journal of marine*

research, 38(4):687–701, 1980.

N Skliris, K Elkalay, A Goffart, C Frangoulis, and J.H. Hecq. One-dimensional modelling of the plankton ecosystem of the north-western Corsican coastal area in relation to meteorological constraints. *Journal of Marine Systems*, 27:337–362, 2001.

Karline Soetart, Peter M.J. Herman, Jack J. Middelburg, Carlo Heip, Claire L. Smith, Paul Tett, and Karen Wild-Allen. Numerical modelling of the shelf break ecosystem: reproducing benthic and pelagic measurements. *Deep-Sea Research II*, 48:3141–4177, 2001.

Karline Soetart, Jack J. Middelburg, Peter M.J. Herman, and Kert Buis. On the coupling of benthic and pelagic biogeochemical models. *Helgoland Marine Research*, 51:173–201, 2000.

JH Steele and EW Henderson. The role of plankton in predation models. *Journal of Plankton Research*, 14(1):157–192, January 1992.

JS Wroblewski. Model of phytoplankton plume formation during variable Oregon upwelling. *Journal of marine research*, 35(2):357–394, 1977.

Informatik og Matematisk Modellering
Danmarks Tekniske Universitet
DK – 2800 Lyngby, Danmark